PHYSICAL REVIEW D **81,** 075012 (2010)

Astrophysical implications of a visible dark matter sector from a custodially warped GUT

Kaustubh Agashe,[1] Kfir Blum,[2] Seung J. Lee,[2] and Gilad Perez[2]

[1]*Maryland Center for Fundamental Physics, Department of Physics, University of Maryland, College Park, Maryland 20742, USA*
[2]*Department of Particle Physics and Astrophysics, Weizmann Institute of Science, Rehovot 76100, Israel*
(Received 17 January 2010; published 20 April 2010)

We explore, within the warped extra dimensional framework, the possibility of finding antimatter signals in cosmic rays (CRs) from dark matter (DM) annihilation. We find that exchange of order 100 GeV radion, an integral part of this class of models, generically results in a sizable Sommerfeld enhancement of the annihilation rate for DM mass at the TeV scale. No *ad hoc* dark sector is required to obtain boosted annihilation cross sections and hence signals. Such a mild hierarchy between the radion and DM masses can be natural due to the pseudo-Goldstone boson nature of the radion. We study the implications of a Sommerfeld enhancement specifically in warped grand unified theory (GUT) models, where proton stability implies a DM candidate. We show, via a partially unified Pati-Salam group, how to incorporate a custodial symmetry for $Z \to b\bar{b}$ into the GUT framework such that a few TeV Kaluza-Klein (KK) mass scale is allowed by electroweak precision tests. Among such models, the one with the smallest $SO(10)$ (fully unified) representation, with $SU(5)$ hypercharge normalization, allows us to decouple the DM from the electroweak gauge bosons. Thus, a correct DM relic density can be obtained and direct detection bounds are satisfied. Looking at robust CR observables, we find a possible future signal in the $\bar{p}/p$ flux ratio consistent with current constraints. Using a different choice of representations, we show how to embed in this GUT model a similar custodial symmetry for the right-handed tau, allowing it to be strongly coupled to KK particles. Such a scenario might lead to an observed signal in CR positrons; however, the DM candidate in this case cannot constitute all of the DM in the Universe. As an aside and independent of the GUT or DM model, the strong coupling between KK particles and tau's can lead to striking LHC signals.

DOI: 10.1103/PhysRevD.81.075012 PACS numbers: 12.60.−i, 95.35.+d

I. INTRODUCTION

In the last few years a host of experiments have provided us with detailed cosmic ray (CR) data in the energy range of 10–1000 GeV [1–11]. The data are interesting for the astrophysics and cosmology communities, enabling them to learn about production and propagation of particles in the Galaxy. They are also of great interest for the particle physics community, due to the anticipation that annihilation of dark matter (DM), possibly consisting of weakly interacting massive particles (WIMPs), would generate an observable signal in the CR data. A lot of model building effort has recently been associated with the PAMELA [1] and ATIC/Fermi/HESS [2–4,11] measurements. Probably the main reason for the excitement is due to a rise in the positron to the total electron flux ratio (positron fraction) in the 10–100 GeV energy range, as measured by PAMELA. The rising positron fraction is in tension with common assumptions regarding the production and propagation of CR electrons and positrons in the Galaxy (see e.g. [12,13], and references therein).

The rising positron fraction,[1] though certainly intriguing, does not necessarily imply an "anomaly" with respect to what could be expected from standard astrophysics as follows: The actual positron intensity does not exhibit an excess when contrasted with model independent calculations [15], which successfully describe the observed abundance of other secondary CR particles, such as antiprotons. Moreover, since measurements of unstable CR isotopes can be used to infer the cooling suppression of positrons at an energy of around 20 GeV, a theoretical estimate for the corresponding positron flux can be derived at that energy [15]. Thus, the combination of the predicted positron flux and the available $e^- + e^+$ data [2,3,5,7–9] yields an independent estimate of the background positron fraction for this energy range. The authors of [15] have compiled the above data and shown that it is, in fact, consistent with the PAMELA measurement, leaving little room for an anomaly. It is, therefore, conceivable that the rising positron fraction may just imply that the currently fashionable diffusion models for CR propagation in the Galaxy are incorrect.

Even within simple diffusion models, the PAMELA result has been argued to be compatible with secondary positrons, provided that the primary electron spectrum is soft [13,16]. Along these lines there are alternative astrophysical interpretations, wherein the positrons are still of secondary origin [17–19]. We note that, at present, all of these astrophysical interpretations require further assessment in order to verify the compatibility of the rising positron fraction with the CR nuclei and antiproton data. In regards to suggested primary injection mechanisms, pulsars have been put forth as astrophysical source candidates (see e.g. [20]), and models of DM annihilation or

[1]See, however, [14] for cautionary notes.

decay have been proposed as a particle physics explanation (see e.g. [21–25]).

A common feature of the DM annihilation models which can account for observable contributions of antimatter CRs is the presence of a large enhancement (''boost'') factor in the annihilation cross section. This feature can be traced back to the Wilkinson Microwave Anisotropy Probe (WMAP) data, which fixes the annihilation cross section at the cosmological epoch to $\langle\sigma v\rangle \sim$ few 10^{-26} cm^3 s^{-1}. For DM mass in the TeV range, the latter number implies that the positron (or other antimatter particle) injection rate lies orders of magnitude below the astrophysical background. One widely studied possibility for obtaining a boost factor of the velocity-weighted current annihilation cross section relative to its cosmological value at freeze-out is the so-called ''Sommerfeld enhancement'' (SE) [26], which originates from DM particles interacting via a light force carrier. Other forms of enhancement have also been studied in the literature (see e.g. [27–29]).

While not currently necessitated by data, it is still an interesting possibility that the observed CR fluxes include a primary component from DM annihilation. Furthermore, in wait of future data release by the PAMELA and upcoming missions [30,31], it is timely to consider theoretically clean observables for indirect detection, such as the antiproton to proton and positron to antiproton flux ratios [15].

In this paper we explore such robust observables using a well-motivated theoretical framework, namely, that of a warped extra dimension *á la* the Randall-Sundrum model (RS1) [32], but with standard model (SM) fields propagating in it. One nice feature of the warped extra dimension framework in light of indirect astrophysics signals is that there is a natural candidate for the force carrier of the SE, namely, the radion, which is an intrinsic component of the theory.[2] It is the degree of freedom corresponding to fluctuations of the size of the extra dimension in a RS-type scenario. The radion mass is, in principle, a free parameter of the theory, but assuming no fine-tuning [and a Kaluza-Klein (KK) scale of $\mathcal{O}(3$ TeV$)$] its mass could vary from $\mathcal{O}(100$ GeV$)$—a limit in which it can be considered as a pseudo-Goldstone boson (PGB)[3]—all the way to the KK scale. The precise radion mass depends on the mechanism which stabilizes the distance between the branes [34–40]. In addition, the radion couplings to other particles are (roughly) given by the mass of those particles in units of the KK scale. Hence, for a TeV scale DM, the radion coupling to the DM pair is $\mathcal{O}(1)$, and a radion mass as large as a few hundred GeV can give a significant SE.

We focus here on a variant of the DM model based on a grand unified theory (GUT) model within this framework [41],[4] where stability of the DM is a spin-off of suppressing proton decay. The DM particle in this model is a SM gauge singlet and a nonstandard GUT partner of the top quark. We incorporate custodial symmetry protection of the Z coupling to bottom quarks [44] into the above existing RS-GUT model, in order to suppress the otherwise large shift in this coupling, and construct several models of this type. For simplicity, we mainly focus on partial unification based on the Pati-Salam group, which captures the major experimental implications; however, full unification is discussed as well.

We also explore the consequences of implementing similar custodial symmetry protection of Z couplings to right-handed (RH) tau's, in order to accommodate the possibility of RH tau's being localized near the TeV end of the extra dimension, and hence having a large coupling to KK particles in this model. In such a scenario, DM annihilation can have large leptonic branching ratios (BRs) via Z'—the extra $U(1)$ of the Pati-Salam group—exchange.[5] It is interesting that such large leptonic BRs can result in indirect detection in CR positron/electrons. We emphasize that, independent of the GUT or DM model, such a possibility, in turn, opens up new doors for searching for KK particles (for example, KK Z) at the LHC through their decay into highly boosted RH tau's, which will be a relatively clean signal with negligible SM background.

We find, however, that models with significant DM-Z' couplings which allow for such exciting astrophysics phenomenology, in general, yield a too-small primordial DM density or are in tension with direct detection bounds. Furthermore, this scenario seems to require very large representations when fully unified into $SO(10)$ and, in any case, it is incompatible with $SU(5)$ normalization of hypercharge. Thus, even the SM level of gauge couplings unification [which is automatic in warped models with $SU(5)$ normalization of hypercharge [45]] is not guaranteed to be maintained.

We hence consider other classes of models, which can be fully unified into not-so-large $SO(10)$ representations, and furthermore preserve the $SU(5)$ normalization of hypercharge. Thus, the SM level of gauge couplings unification is maintained, and even unification with precision comparable to the supersymmetric SM might be possible, as in Ref. [46]. It is quite interesting that this model actually predicts vanishing DM-Z' coupling, so that the above relic

[2]Based on AdS/CFT correspondence, this nice feature of the radion as a mediator of SE is *dual* to dilaton exchange in 4D CFT theories of electroweak symmetry breaking, with an appropriate DM candidate. Reference [33] considered the dilaton as a messenger between the SM and the dark sector, but did not study the SE from dilaton exchange.

[3]However, unlike other PGB's, the radion can have sizable nonderivative couplings (required for Sommerfeld enhancement) even in the GB limit.

[4]Based on the above discussion, it is clear that radion mediated SE might also be relevant for *other* RS-type scenarios with a DM candidate [42,43].

[5]Recall that the DM is a SM singlet, so that KK exchange of SM gauge fields is not allowed at leading order.

density and direct detection constraints are all satisfied, albeit (as a corollary) this does not lead to exciting astrophysics signals in the positron/electron channel. Note, however, that custodial $Z \to \tau\bar{\tau}$ symmetry protection can still be implemented in this GUT model, so that the exciting LHC phenomenology associated with tau's is possible. Finally, we would like to mention that Refs. [47,48] studied indirect detection of DM in a version of the above model without custodial protection for $Zb\bar{b}$ coupling and without including the Sommerfeld enhancement due to the radion exchange.

The outline of the rest of the paper is as follows. We begin in Sec. II with a description of the model, which is a modified version of the warped extra dimension DM model of Ref. [41]. The unification scheme and custodial symmetry protection mechanism are detailed in Sec. III. In Sec. IV we discuss implications for cosmology and astrophysics. We explore the SE arising in our framework with a (light) radion, proceeding to calculate the DM relic density and direct detection cross sections. The parameter space compatible with WMAP observations and Cryogenic Dark Matter Search (CDMS) bounds is delimited. A set of benchmark models within this allowed parameter space is defined, in which a large SE factor is a natural consequence of the setup. Particle and astrophysics aspects of DM annihilation are discussed. In Sec. V we briefly discuss the radion-related collider signals at the LHC. Our conclusions are drawn in Sec. VI. We leave certain details of the particle physics model and of the astrophysics calculations to Appendixes A and B.

II. THE MODEL

We first present a review of the general warped extra dimensional framework and then of the DM model within it. For a review and further references, see [49]. The reader interested only in the particle content of the model and the couplings relevant for signals in cosmic ray experiments can skip to Tables IV, V, and VI and the comments listed there.

A. SM fields in the bulk of warped extra dimensions

The RS1 framework consists of a slice of anti–de Sitter space in five dimensions (AdS_5), where the warped geometry naturally generates the Planck-weak hierarchy as follows [32]. The 4D graviton, i.e., the zero mode of the 5D graviton, is automatically localized at one end of the extra dimension (hence called the Planck/UV brane). If the Higgs sector is localized at the other end (hence called the TeV/IR brane),[6] then the UV cutoff for quantum corrections to the Higgs mass can be $\sim$(TeV), whereas the 4D gravitational coupling strength is simultaneously being set by the usual Planck scale, $M_{\rm Pl} \sim 10^{18}$ GeV. Such a hierarchy of mass scales at the two ends of the extra dimension is stable against quantum corrections in the warped geometry, where the effective 4D mass scale (including the UV cutoff) is dependent on the position in the extra dimension. Specifically, TeV $\sim M_{\rm Pl} e^{-k\pi R}$, where k is the AdS_5 curvature scale and R is the proper size of the extra dimension. The crucial point is that the required modest size of the radius (in units of the curvature radius), i.e., $kR \sim 1/\pi \log(M_{\rm Pl}/\text{TeV}) \sim 10$, can be stabilized with only a corresponding modest tuning in the fundamental or 5D parameters of the theory [34,40]. Remarkably, the correspondence between AdS_5 and 4D conformal field theories (CFT) [51] suggests that the scenario with a warped extra dimension is dual to the idea of a composite Higgs in 4D [50,52].

In the original RS1 model, it was assumed that the rest of the SM, i.e. gauge and fermion, fields are also localized on the TeV brane (just like the Higgs). Such a scenario does not have a built-in explanation for the hierarchy between quark and lepton masses and mixing angles (flavor hierarchy). In addition, the scenario generically also has flavor and proton stability problems as follows. The (effective) cutoff for the *entire* SM (i.e., not just the Higgs) is of $\mathcal{O}$ (TeV) in this case, so that the higher-than-dimension-4 SM operators induced by the UV completion of RS1 will lead to too-large flavor changing neutral currents (FCNC's) and too-rapid proton decay: Recall that such operators have to be suppressed by, at least, $\mathcal{O}(10^5)$ TeV (if they violate CP in addition) and $\sim 10^{15}$ GeV, respectively, to be consistent with the data. The above argument suggests that a similar problem would be present for the electroweak (EW) sector, a manifestation of the little hierarchy problem.

1. Solution to flavor puzzle and problem

It was realized that with SM fermions propagating in the bulk, i.e., arising as zero modes of 5D fermions, we can account for the flavor hierarchy as well [53,54]. The idea is that the effective 4D Yukawa couplings of the SM fermions are given by a product of the fundamental 5D Yukawa couplings and the overlap of the profiles (of the SM fermions and the Higgs) in the extra dimension. Moreover, vastly different profiles in the extra dimension for the SM fermions, and hence their hierarchical overlaps with Higgs, can be easily obtained by small variations in the 5D fermion mass parameters. Thus, hierarchies in the 4D Yukawa couplings can be generated without any (large) hierarchies in the fundamental 5D parameters (5D Yukawa couplings and 5D mass parameters for fermions).

As a bonus, the above-mentioned flavor problem is also solved as follows. Based on the above discussion, we can see that light SM fermions are chosen to be localized near the Planck brane in such a way that the effective cutoff for them is $\gg$ TeV. In more detail (this discussion will be

[6] In fact, with SM Higgs originating as the 5th component of a 5D gauge field (A_5), this is automatically so [50].

useful in what follows), the contribution to the four-fermion operators from the physics at the cutoff dominantly comes from the region near the TeV brane [where the effective cutoff is of course of $\mathcal{O}$ (TeV)], but the operators are further suppressed by the profile of the SM fermions near the TeV brane. Since the same profiles dictate the 4D Yukawa couplings, we see that four-fermion operators have a coefficient $\sim 1/\mathrm{TeV}^2 \times (4D\,\mathrm{Yukawa})^2$, which is sufficient to suppress FCNC's:

$$\begin{aligned}&\psi^4_{\mathrm{SM}}/\mathrm{TeV}^2\,(\text{SM on TeV brane})\\ &\quad\to \psi^4_{\mathrm{SM}}/\mathrm{TeV}^2 \times \text{profiles at TeV brane (SM in bulk)}\\ &\quad\sim \psi^4_{\mathrm{SM}}/\mathrm{TeV}^2 \times (4D\ \mathrm{Yukawa})^2. \qquad (1)\end{aligned}$$

As a corollary, the SM gauge fields must also propagate in the bulk (hence the scenario is called "SM in the bulk"). Thus, the couplings of SM fermions (with different profiles) to gauge KK modes are nonuniversal, resulting in flavor violation from exchange of these KK modes [55]. However, there is a built-in analog of the Glashow-Iliopoulos-Maiani mechanism of the SM in this framework [54,56,57] which suppresses FCNC's. Namely, the nonuniversalities in couplings of SM fermions to KK modes are of the size of 4D Yukawa couplings since KK modes have a similar profile to the SM Higgs; i.e., gauge KK modes are localized near the TeV brane. Thus, even though the gauge KK mass is of $\mathcal{O}$ (TeV), FCNC's from their exchange can be adequately suppressed.[7] Similarly, the KK modes induce effects on electroweak precision tests (EWPT), which can be brought under control by suitably imposed custodial symmetries [44,61].

2. Baryon symmetry

Satisfying the constraints from the nonobservation of proton decay requires, however, the new physics mass scale to be generically of $\mathcal{O}(10^{15})$ GeV, so that the Yukawa-type suppression of cutoff effects on top of a $\mathcal{O}$ (TeV) scale, discussed above, is not enough in this case. A simple solution is to impose a gauged[8] baryon-number symmetry, denoted by $U(1)_B$, in the bulk and to break it (arbitrarily) on the Planck brane, so that the "-would-be" zero-mode gauge boson is projected out. Thus, proton decay operators can originate only on the Planck brane, where they are adequately (i.e., Planck scale which is the cutoff there) suppressed:

$$q^3 l/\mathrm{TeV}^2\,(\text{SM on TeV brane}) \to q^3 l/M^2_{\mathrm{Pl}}\,(\text{SM in bulk}). \qquad (2)$$

B. Dark matter from proton stability in GUT

Extending the bulk gauge symmetry from the SM to a GUT is motivated by the resulting SUSY-level precision gauge coupling unification [46], in addition to an explanation for the quantized hypercharges of the SM fermions.

However, the extra gauge bosons in the GUT—for example, X, Y in the case of $SU(5)$—have their KK excitations [with a mass of $\mathcal{O}$ (TeV)] localized near the TeV brane (even if their would-be zero modes can be decoupled by suitable breaking of the GUT). Hence, if the SM quarks and leptons are *grand unified* as well, i.e., they arise as zero modes from the same 5D multiplet in a GUT representation, then the X and Y exotic gauge KK modes will mediate proton decay with only Yukawa suppression [beyond their $\mathcal{O}$ (TeV) mass] which is clearly not sufficient.

1. Split multiplets

The solution is to invoke "split" multiplets; namely, we break the GUT group down to the SM by boundary conditions (on the Planck brane so that gauge coupling unification still works). We can then choose SM quarks and leptons to be zero modes of two *different* 5D multiplets in a GUT representation. The extra (i.e., would-be) zero modes with SM gauge quantum numbers of leptons and quarks, respectively, from the two 5D multiplets can be projected out by the boundary condition; i.e., these fields have only *massive* KK excitations. In this way, the X, Y gauge bosons cannot couple SM quarks to SM leptons (again such a coupling can only arise if SM quarks and SM leptons are contained in the same 5D multiplet): see Fig. 1.

However, higher-order effects can "undo" the splitting of quark and lepton multiplets, so that proton decay can strike again—for example, brane-localized mass terms can mix the (KK) leptons from the "quark" multiplet (i.e., which contains a quark zero mode) with the zero-mode lepton from the other (lepton) multiplet, and similarly mix (KK) quarks from the lepton multiplet with the quark zero mode from the quark multiplet. In any case, we still have to contend with cutoff effects giving proton decay. A simple way out is to impose a $U(1)_B$ gauge symmetry in the bulk, as discussed in the case of the non-GUT model. Specifically, the *entire* 5D quark (lepton) multiplet, including the KK leptons (quarks) contained in it, are assigned $B = 1/3$ (0).

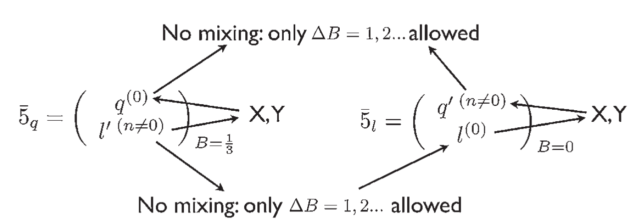

FIG. 1. Split multiplets.

[7] A residual "little *CP* problem" [58] is still present [57,59] in the above scenario, which can be amended by various alignment mechanisms [58,60].

[8] Global symmetries are expected to be violated by quantum gravity effects.

2. Z_3 symmetry

Unlike in the non-GUT model, a (*discrete*) subgroup of $U(1)_B$ has to be preserved during the breaking of the $U(1)_B$ on the Planck brane, in order to prevent mixing between the KK leptons from the quark multiplet with the lepton zero modes from the lepton multiplet (and thus avoid catastrophic proton decay). For example, it is possible to require that the $U(1)_B$ symmetry is only broken by scalar fields with integer charges; i.e., only $\Delta B = 1, 2, \ldots$ operators are allowed. Thus, the above-mentioned mixing of "wrong" (i.e., KK) leptons (or quarks) with $B = 1/3$ (or 0) with correct zero modes with $B = 0$ (or $1/3$) is forbidden (see Fig. 1), even though four-fermion proton decay operators, albeit safe due to the Planckian suppression, are allowed.

The crucial observation is that, as a corollary, the GUT partners of the SM quarks and leptons, i.e., the (KK) leptons (quarks) from the quark (lepton) multiplet, cannot decay into purely SM particles due to their "exotic" baryon-number assignment. Explicitly, the extra particles in the GUT model (including X, Y gauge bosons) are charged under the following Z_3 symmetry:

$$\Phi \rightarrow e^{2\pi i(((\alpha - \bar{\alpha})/3) - B)}\Phi \tag{3}$$

(where α, $\bar{\alpha}$ are the number of color, anticolor indices on Φ), whereas the SM particles—having correct combinations of color and baryon number—are neutral under it. Thus, the lightest Z_3 charged particle (dubbed "LZP") is stable.

In Ref. [41], an $SO(10)$ model with canonical representations for SM fermions, i.e., in **16**, was presented. It was shown that the SM singlet (RH neutrino) partner of t_R[9] can be the LZP and is in fact a WIMP, and therefore a good dark matter candidate: a spin-off of suppressing proton decay (analogous to R parity in supersymmetry).[10]

III. PARTIALLY AND FULLY UNIFIED CUSTODIAL MODELS

In models with the canonical/minimal choice of EW quantum numbers, the shift in $Zb\bar{b}$ resulting from exchange of KK modes is typically (a bit) larger than that allowed by EWPT. This shift results in a $\mathcal{O}(5\text{ TeV})$ lower bound on the KK scale, which implies a rather severe little hierarchy problem. A custodial symmetry to protect such a shift in $Zb\bar{b}$ was proposed in Ref. [44], and it requires noncanonical EW quantum numbers.

Here, we incorporate such a custodial symmetry in the warped GUT DM model of Ref. [41], presenting several models of this type. For simplicity, we mainly work with a partially unified, i.e., Pati-Salam, gauge group and comment on full unification into $SO(10)$ on a case by case basis. Note that there is no proton decay from the exchange of X, Y-type GUT gauge bosons in the Pati-Salam model, so there is no motivation for incorporating split multiplets and hence for the existence of DM of this type in this case. However, we always have full unification into $SO(10)$, where DM emergence is a spin-off of proton stability as mentioned above, in the back of our minds.

It is interesting that such a symmetry can also be extended to leptons in order to protect the shift in the Z coupling to leptons. Thus, leptons (in particular, τ) can be localized closer to the TeV brane, resulting in larger (than canonical) couplings of gauge KK modes to τ. A significant DM annihilation to τ via exchange of KK gauge bosons, therefore, might be possible, which may be relevant for the PAMELA rise (or future signals). As further discussed below, this possibility is typically in tension with the observed DM relic density and with direct detection limits.

Finally, although we focus here on models where the DM is a SM gauge singlet GUT partner of t_R, it is worth noting that the DM could also be the GUT partner of $(t, b)_L$ instead, depending on details such as the proximity of these profiles to the TeV brane. We defer the study of such a possibility to the future.

A. Canonical

Just to get oriented, the canonical choice for representations under the Pati-Salam group, i.e., $SU(4)_C \times SU(2)_L \times SU(2)_R$, are in Table I.[11] Namely, left-handed (LH) SM fermions, i.e., $SU(2)_L$ doublet quarks and leptons, are $SU(2)_R$ singlets with $T_{3R} = 0$. RH quarks and leptons, i.e., $SU(2)_L$ singlets, are $SU(2)_R$ doublets with $T_{3R} = \pm 1/2$ for RH up quarks (or RH neutrinos) and RH down quarks (or RH charged leptons). The SM hypercharge is then given by

$$Y = T_{3R} - \sqrt{2/3}X, \tag{4}$$

where X are the charges under the non-QCD $U(1)$ generator present in $SU(4)_c$, i.e., $SU(4)_c \sim SU(3)_c \times U(1)_X$. We have chosen $X = \text{diag}\sqrt{3/8}(-1/3, -1/3, -1/3, 1)$ when acting on **4** of $SU(4)_c$ such that the normalization for this generator acting on **4** of $SU(4)_c$ is $\text{Tr}X^2 = 1/2$. This combination of T_{3R} and X corresponds to the $SU(5)$ normalization of hypercharge when fully unified into $SO(10)$. Thus this model (at the least) maintains the SM level of unification of couplings, even in the context of a warped extra dimension.

Thus, we have the breaking pattern $SU(4)_c \times SU(2)_R \rightarrow SU(3)_c \times U(1)_Y$ achieved by the boundary condition on the Planck brane. The Pati-Salam group is preserved by

[9] The t_R multiplet being the one giving the LZP follows from its profile being closest to the TeV brane.

[10] In addition to DM, other GUT partners could also give interesting signals (see e.g. [41,62]).

[11] Of course, we can invoke split multiplets so that there can be two multiplets—one for quarks and one for leptons—of each type in the table.

TABLE I. Canonical representations for SM fermions and Higgs; the subscripts denote the $\sqrt{8/3}\,X$ charge.

	$SU(4)_c \sim SU(3)_C \times U(1)_X$	$SU(2)_L$	$SU(2)_R$
LH	$\mathbf{4} \sim \mathbf{3}_{-1/3} + \mathbf{1}_1$	**2**	**1**
RH	$\mathbf{4} \sim \mathbf{3}_{-1/3} + \mathbf{1}_1$	**1**	**2**
H	**1**	**2**	**2**

boundary conditions on the TeV brane [of course, the Higgs vacuum expectation value breaks $SU(2)_L \times SU(2)_R \to SU(2)_V$]. The gauge field that corresponds to the combination of T_{3R} and X which is orthogonal to the hypercharge will be denoted by Z'. The couplings to Z' are then given by (up to an overlap factor denoted below by a) $(g_R/\cos\theta')(T_{3R} - Y\sin^2\theta')$, where $\sin^2\theta' \equiv (\frac{3}{2}g_4^2)/(\frac{3}{2}g_4^2 + g_R^2)$ and g_R, g_4 are the "4D" couplings of the $SU(4)_C$ and $SU(2)_R$ gauge groups, respectively. [Obviously the normalized $U(1)_X$ gauge coupling is the same as the $SU(4)_c$ one.]

Note that, due to the Pati-Salam group being only a partial unification of the SM gauge groups, the $SU(2)_R$ and $SU(4)_c$ gauge couplings are unrelated so that $\sin^2\theta'$ is a free parameter. However, it was shown in Ref. [46] that a $SO(10)$-type completion of the Pati-Salam group, i.e., full unification of SM gauge groups, is very well motivated due to the SUSY-level precision of the gauge coupling unification. With this result in mind, we can set $g_4 = g_R$ to find $\sin^2\theta' = 3/5$.

B. Custodial Pati-Salam model

As outlined above, we begin by constructing a model with custodial symmetry for $Zb\bar{b}$ based on partial unification, namely, the Pati-Salam gauge group: $SU(4)_C \times SU(2)_L \times SU(2)_R$. We later discuss how to fully unify it. For the implementation of the custodial protection for $Zb\bar{b}$ coupling, the required charges are

$T_{3R} = -1/2$ for $(t, b)_L$ and thus $T_{3R} = 0, -1$ for t_R and b_R to obtain the top and bottom masses,[12] respectively.

Thus, we must modify the Pati-Salam representations. Moreover, the $SU(2)_L$ and $SU(2)_R$ 5D gauge couplings must be equal.

However, the above requirement does not completely fix the model. Below, we first discuss the relevant parameters left over and then describe a variety of models with specific choices of these parameters.

1. Composite charge leptons

Once we resort to noncanonical representations, we can choose

$T_{3R} = 0$ for τ_R (and other RH charged leptons) in order to provide custodial protection for its coupling to Z as well.

[12]In the model where top and bottom masses are obtained from the same 5D $(t, b)_L$ multiplet.

In this way, τ_R can be localized very close to the TeV brane[13]; i.e., we can contemplate larger couplings of KK τ_R to gauge KK modes (in particular, Z'). Since, via AdS/CFT correspondence, such a scenario is dual to τ_R being a composite particle of 4D strong dynamics, we will refer to this feature as "composite" τ_R.[14] Then we must choose $T_{3R} = +1/2$ for $(\nu, \tau)_L$ to obtain charged lepton masses.

One may wonder whether the possibility of having a composite τ_R is constrained by precision tests. For instance, virtual KK Z boson exchange will generate four-fermion operators involving τ_R and other SM fermions. In our case the dominant constraint comes from the $(\bar{e}\gamma^\mu e) \times (\bar{\tau}\gamma_\mu \tau_R)$ operator since the couplings of KK Z bosons to electrons are vectorlike in nature, whereas the tau's are RH as discussed above. Using the LEP bounds on such contact interactions from [63], we find that the effective scale suppressing this higher dimension operator should be at least 3 TeV. In our case, the KK Z coupling to τ_R is (roughly) given by $\sim g_Z\sqrt{k\pi R}$, while the electron coupling is $\sim g_Z/\sqrt{k\pi R}$, which gives roughly a coefficient of $1/(4\ \text{TeV})^2$ for this operator for a 3 TeV KK mass scale, and hence is consistent with the bounds. However, with a composite τ_R, constraints from lepton flavor violation might still be an issue which can be addressed by gauging (at the 5D level) the flavor symmetries [60].

2. DM couplings to Z'

Of particular importance are obviously the representation and hence coupling of the DM candidate, ν'. Since the couplings of Z' are, in general, of the same form as the canonical model (albeit with a different $\sin\theta'$) and the DM is a SM gauge singlet ($Y = 0$), its coupling to Z' is proportional to T_{3R}; i.e., the coupling of ν' to Z' is vanishing (nonvanishing) for $T_{3R}^{\nu'} = 0$ ($\neq 0$). In the case $T_{3R}^{\nu'} = 0$, the DM coupling to the SM Z (of course induced by higher-order effects) is also custodially protected [44]. Obviously, the model's phenomenology differs qualitatively depending on whether the DM couples to Z' (and Z) or not, so that a crucial choice is

$T_{3R}^{\nu'} \neq 0$ vs $T_{3R}^{\nu'} = 0$.

In the following sections we discuss two specific models (two more are given in Appendix A), which demonstrate the essential differences. Because of the fact that our DM is localized near the TeV brane (just like other KK's), a nonvanishing $T_{3R}^{\nu'}$ would imply a sizable DM-Z' coupling. This case tends to yield a too-large annihilation cross

[13]In order to obtain the charged lepton mass hierarchy, e_R and μ_R might have to be localized farther away from the TeV brane than the τ_R.

[14]Note that the custodial symmetry cannot protect a shift in Z coupling to LH charged leptons and LH neutrinos *simultaneously*, since we require $T_{3R} = T_{3L}$ for this purpose and LH charged leptons and LH neutrinos obviously have different T_{3L}, but the same T_{3R}.

section via Z' exchange into electroweak gauge bosons/top quarks, and hence typically a too-low relic density, unless the DM is of $\mathcal{O}(100)$ GeV in which case direct detection from Z exchange becomes a strong constraint. Of course, if in addition τ_R is a composite, then the DM annihilation into τ_R's (which do couple to Z') could be significant, which could be interesting for indirect cosmic ray positron/electron signals.

As we shall see later, it is quite remarkable that our model with the smallest fully unified, i.e., $SO(10)$, representations actually predicts $T_{3R}^{\nu'} = 0$. Thus, it leads to vanishing coupling of the DM to Z' and SM Z, making it compatible with the observed DM relic density and direct detection bounds.

Finally, in the case where $T_{3R}^{\nu'} = 0\,(\neq 0)$ we also require $X^{\nu'} = 0\,(\neq 0)$ in order to obtain $Y^{\nu'} = 0$ (again, in general, the hypercharge is a combination of T_{3R} and X, but is different than in the canonical model).

C. Model I (a): $T_{3R}^{\nu'} \neq 0$ and custodial symmetry for leptons

One possible choice of noncanonical Pati-Salam representations satisfying the above conditions for cosmic ray signals in positrons/electrons is given in Table II. The SM hypercharge is then given by

$$Y = T_{3R} + \sqrt{1/6}X, \tag{5}$$

and the DM and t_R arise from a **35** of $SU(4)$. The couplings to Z' are then given by

$$\frac{g_{LR}}{\cos\theta'}(T_{3R} - Y\sin^2\theta')$$

as before, but with $\sin^2\theta'_{\mathbf{35}} \equiv (6g_4^2)/(6g_4^2 + g_{LR}^2)$, instead of the canonical value due to the modified combination of T_{3R} and X entering the hypercharge [note that g_R from before is replaced by g_{LR} due to the equality of $SU(2)_{L,R}$ couplings]. $\sin^2\theta'$ is a free parameter at the level of the Pati-Salam gauge group. We will leave the task of a detailed completion of this model into $SO(10)$-type full unification, including calculation of the resulting gauge coupling unification in this model, for future work. Here, we simply note a few features of a potential unification into $SO(10)$. First, such an extension seems to require $SO(10)$

TABLE II. An example of a model with custodial representations for b_L and RH charged leptons, with nonvanishing $\nu'\bar{\nu}'Z'$ coupling (see Table V); the subscripts denote the $\sqrt{8/3}\,X$ charge.

	$SU(4)_c \sim SU(3)_C \times U(1)_X$	$SU(2)_L$	$SU(2)_R$
t_R, ν'	$\mathbf{35} \sim \mathbf{3}_{8/3}, \mathbf{1}_4 \ldots$	**1**	**3**
$(t, b)_L$	$\overline{\mathbf{35}} \sim \mathbf{3}_{8/3}, \ldots$	**2**	**2**
τ_R	$\overline{\mathbf{35}} \sim \mathbf{1}_{-4}, \ldots$	**1**	**1**
$(\nu, \tau)_L$	$\overline{\mathbf{35}} \sim \mathbf{1}_{-4}, \ldots$	**2**	**2**
b_R	$\mathbf{35} \sim \mathbf{3}_{8/3}, \ldots$	**1**	**3**
H	**1**	**2**	**2**

representations larger than **560** [64]. Moreover, even if we find such a representation, the normalization of the hypercharge above is not the usual $SU(5)$ one, so this model does not even maintain the SM level of unification of couplings.

However, a loop-level matching of the 5D gauge couplings to the observed QCD and $SU(2)_L$ ones with the assumption of small tree-level brane kinetic terms gives $g_{LR} \approx g_4$ [just like the canonical $SO(10)$ case]. Based on this observation, we can choose $g_{LR} \approx g_4$ (i.e., $\sin^2\theta' \approx 6/7$) as a ''benchmark'' value for this Pati-Salam model. It is crucial to realize that the above model is just one choice satisfying the conditions of custodial symmetry for the $Zb\bar{b}$ coupling, so that the value $T_{3R} = -1$ (giving $Y = 0$) for ν' (and similarly the value of $\sin^2\theta'$, even with the assumption of $g_{LR} \approx g_4$) is not unique: See the model below and the two models in Appendix A.

D. Model II: Smallest full unification

We shall now construct a Pati-Salam model based on the **15** representation of $SU(4)$, and show that it is compatible with full unification into $SO(10)$.[15] The model also has $SU(5)$ normalization for the hypercharge, and it predicts vanishing $T_{3R}^{\nu'}$ and hence DM coupling to Z'/Z.

The Pati-Salam model is shown in Table III. It can be fully unified into the following $SO(10)$ representations: **45** for t_R and b_R, **120** for $(t, b)_L$, and the canonical, i.e., **16**, for leptons. So, RH charged leptons are not protected by the custodial symmetry, but the model can be modified easily to include this feature: for example, LH and RH leptons being $(\mathbf{10}, \mathbf{2}, \mathbf{2})$ and $(\mathbf{10}, \mathbf{1}, \mathbf{1})$ under $SU(4)_c \times SU(2)_L \times SU(2)_R$, respectively, which fit into **210** and **120**, respectively, of $SO(10)$. Moreover, the hypercharge normalization

$$Y = T_{3R} - \sqrt{\tfrac{2}{3}}X \tag{6}$$

is the *same* as in $SU(5)$, so this model maintains SM-level unification of couplings when fully unified into $SO(10)$.

Vanishing coupling of Z' to ν' pair ($T_{3R}^{\nu'} = 0$)

Note that the X charge of ν' vanishes (see Table III) for this choice of the t_R representation, so the $\nu'\bar{\nu}'Z'$ and $\nu'\bar{\nu}'Z$ couplings vanish. Thus, this case might be uninteresting for indirect searches for DM annihilation in cosmic ray positrons/electrons, *irrespective* of custodial symmetry for RH charged leptons—that is why we simply chose the canonical representations for leptons in Table III. However, as shown below, it may lead to an observed future signal due to anomalously large antiproton flux in the hundreds of GeV region, and it has the benefit of yielding a correct DM relic abundance. And, with the custodial symmetry for RH leptons, LHC signals related to composite τ_R become a possibility.

[15] See also Ref. [65].

TABLE III. An example of a model with custodial representations for b_L, which results in the simplest full unification. Charged leptons are not protected by the custodial symmetry, and the $\nu' \bar{\nu}' Z'$ coupling vanishes (see Table VI). The subscripts denote the $\sqrt{8/3}\,X$ charge.

	$SU(4)_c \sim SU(3)_C \times U(1)_X$	$SU(2)_L$	$SU(2)_R$
t_R, ν'	$\mathbf{15} \sim \mathbf{3}_{(-4)/3}, \mathbf{1}_0 \ldots$	**1**	**1**
$(t, b)_L$	$\mathbf{15} \sim \mathbf{3}_{(-4)/3}, \ldots$	**2**	**2**
τ_R	$\mathbf{4} \sim \mathbf{1}_1, \ldots$	**1**	**2**
$(\nu, \tau)_L$	$\mathbf{4} \sim \mathbf{1}_1, \ldots$	**2**	**1**
b_R	$\mathbf{15} \sim \mathbf{3}_{(-4)/3}, \ldots$	**1**	**3**
H	**1**	**2**	**2**

The couplings to Z' are then given by $(g_{LR}/\cos\theta') \times (T_{3R} - Y \sin^2\theta')$ as before, but with $\sin^2\theta'_{15} \equiv (\frac{3}{2} g_4^2)/(\frac{3}{2} g_4^2 + g_{LR}^2)$ as in the canonical case.

E. Summary of model characterization

The relevant particle content and couplings are summarized in Tables IV, V, and VI for the partial (fully) unifiable models, respectively. A few comments about the tables are in order:

(i) ν' is the SM singlet (i.e., with quantum numbers of a RH neutrino) GUT partner of t_R,[16] but with (exotic) baryon number of 1/3. ν'_R denotes its RH chirality and has a profile localized near the TeV brane (like for any other KK mode), irrespective of the bulk mass (c) parameter for this GUT multiplet[17] which dictates the profile of t_R.

(ii) Following the notation of Ref. [41], $\hat{\nu}'_R$ denotes the Dirac partner (*left*-handed) of ν'_R.[18] Its profile does depend on c for t_R in such a way that it moves farther away from the TeV brane as t_R gets closer to the TeV brane—the ν' mass ($\propto$ this overlap) decreases in this process.

(iii) X_s (mostly relevant for the unifiable model with no DM-Z' coupling) and Z' (relevant for the partially unified model where DM-Z' coupling controls the resulting relic density) are, respectively, the non-Abelian and $U(1)$ gauge bosons (beyond gluons) contained in $SU(4)_c$ and have masses (almost) the same as those of the KK modes of the SM gauge bosons (denoted by $M_{\rm KK}$).

(iv) Neglecting TeV brane-localized kinetic terms for gauge fields, the couplings can be conveniently expressed (as in the middle columns of Tables V and VI) in units of $g_{4\rm D}\sqrt{k\pi R} \equiv g_{5\rm D}\sqrt{k}$, where $g_{5\rm D}$ is the 5D gauge coupling (of mass dimension $-1/2$) such that $g_{4\rm D}$ is the coupling of the (would-be, in some cases) zero mode (and hence is volume suppressed compared to $g_{5\rm D}$).

(v) The custodial symmetry for Z couplings to fermions requires the two $SU(2)$ 5D couplings to be equal, but the $SU(4)_C$ coupling is unrelated to it. Hence, there appear two $g_{4\rm D}$'s in the tables: g_{LR} for the two $SU(2)$ groups and g_4 for the $SU(4)$ group.

(vi) $g_{4\rm D}$'s cannot always be *equated* to the SM gauge couplings, since the relation between the two couplings depends on the presence of tree-level UV brane kinetic terms and also loop corrections. A detailed analysis is left for future work, but here we can choose each of the $g_{4\rm D}$'s to be (independently) roughly between the SM hypercharge and QCD couplings, i.e., $0.35 \lesssim g_{LR}, g_4 \lesssim 1$.

(vii) The a factors in the middle columns of Tables V and VI come from overlap of wave functions in the extra dimension of the involved modes. Specifically, for a coupling of three (usual) KK modes (which are localized near the TeV brane), the overlap gives $a \sim 1$. Then, each time we replace a KK mode by a SM/zero mode, we incur a "cost" of $\sqrt{a_{\rm SM}}$, which is roughly the *ratio* of the profile of a SM fermion/zero mode at/near the TeV brane to that of a KK fermion (or, equivalently, the degree of "compositeness" of these SM fermions in the dual CFT description).

(viii) Similarly, $\sqrt{a_{\hat{\nu}'_R}}$ is the degree of compositeness of $\hat{\nu}'_R$, i.e., the ratio of its profile near the TeV brane to that of a usual KK fermion (which is localized near the TeV brane). With ν'_R being fully composite (i.e., localized near the TeV brane), the particular appearance of $\sqrt{a_{\hat{\nu}'_R}}$ in the table is thus explained.

(ix) We require $\sqrt{a_{t_R} a_{(t,b)_L}} \sim 1/Y_{\rm KK}$, such that we can obtain a top Yukawa—given by $Y_{\rm KK}\sqrt{a_{t_R} a_{(t,b)_L}}$—of 1: Here, $Y_{\rm KK}$ is the coupling of two KK fermions to the Higgs, and we require it to be smaller than $\sim 1/7$, to allow ~ 3 KK modes in the 5D effective field theory.

(x) The mixing angle $\sin^2\theta' \equiv (6g_4^2)/(6g_4^2 + g_{LR}^2)$ appearing in Z' couplings is a free parameter (since

TABLE IV. Particle content relevant for DM (in)direct detection.

SM	t_R, $(t, b)_L$, τ_R, μ_R, W, Z, h
Non-SM	**Comments (quantum numbers)**
ν'	DM: exotic RH ν (SM singlet) with $B = 1/3$
ϕ	Radion (scalar with Higgs-like coupling to SM)
Z'	Extra/non-SM $U(1)$ in GUT
X_s	Leptoquark GUT gauge boson

[16] Since, with custodial protection of $Zb\bar{b}$ coupling, $(t, b)_L$ can also be close to the TeV brane, it is possible that the LZP comes from this multiplet instead of t_R. The analysis for the two cases is similar.

[17] We neglect any GUT breaking here in the 5D fermion mass parameters within a GUT multiplet, unlike Ref. [41] where small splittings of this type were allowed.

[18] ν'_L was used in Ref. [41] for the $SU(2)_L$ doublet from the $(t, b)_L$ multiplet.

TABLE V. Couplings relevant for DM annihilation in the model with custodial symmetry for $Zb\bar{b}$ and RH charged leptons, with nonvanishing $\nu'\bar{\nu}'Z'$ coupling (see Table II): The value of $\sin^2\theta'$ is 6/7, and note that $T_{3R}^{\nu'} = 1$.

Coupling	Value (in units of $g_{LR}\sqrt{k\pi R}$)	Comments
$\bar{\nu}'_R\gamma_\mu Z'^\mu \nu'_R$	$-a_{\nu'_R}\cos^{-1}\theta'$	$a_{\nu'_R} \sim 1$
$\bar{\hat{\nu}}'_R\gamma_\mu Z'^\mu \hat{\nu}'_R$	$-a_{\hat{\nu}'_R}\cos^{-1}\theta'$	$a_{\hat{\nu}'_R} \sim (\frac{m_{\nu'}}{M_{\rm KK}})^2$
$\bar{t}_R\gamma_\mu Z'^\mu t_R$	$-\frac{2}{3}a_{t_R}\cos^{-1}\theta'\sin^2\theta'$	$a_{t_R} \lesssim 1$
$\overline{(t,b)}_L\gamma_\mu Z'^\mu (t,b)_L$	$a_{(t,b)_L}\cos^{-1}\theta'(-\frac{1}{2}-\frac{1}{6}\sin^2\theta')$	$a_{(t,b)_L} \lesssim 1$ such that $\sqrt{a_{t_R}a_{(t,b)_L}} \sim \frac{1}{Y_{\rm KK}} \sim \frac{1}{7}$
$\overline{(\nu,\tau)}_L\gamma_\mu Z'^\mu (\nu,\tau)_L$	$a_{(\nu,\tau)_L}\cos^{-1}\theta'(\frac{1}{2}+\frac{1}{2}\sin^2\theta')$	$a_{(\nu,\tau)_L} \lesssim \frac{1}{10}$
$\bar{\tau}_R\gamma_\mu Z'^\mu \tau_R$	$a_{\tau_R}\cos^{-1}\theta'\sin^2\theta'$	$a_{\tau_R} \lesssim 1$
$\bar{b}_R\gamma_\mu Z'^\mu b_R$	$a_{b_R}\cos^{-1}\theta'(-1+\frac{1}{3}\sin^2\theta')$	$a_{b_R} \lesssim \frac{1}{10}$
$Z_{\rm long}Z'_\mu h$	$a_{Z'H}\frac{\cos\theta'}{2}(p^\mu_{Z_{\rm long}} - p^\mu_h)$	$a_{Z'H} \sim 1$
$W^+_{\rm long}Z'_\mu W^-_{\rm long}$	$a_{Z'H}\frac{\cos\theta'}{2}(p^\mu_{W^+_{\rm long}} - p^\mu_{W^-_{\rm long}})$	$a_{Z'H} \sim 1$
$\bar{\nu}'_R\hat{\nu}'_R\phi$ (radion)	$\frac{m_{\nu'_R}}{\Lambda_r}$ (no $g_{LR}\sqrt{k\pi R}$)	$\Lambda_r \equiv \sqrt{6}M_{\rm Pl}e^{-k\pi R}$

TABLE VI. Couplings relevant for DM annihilation in the simplest fully unifiable custodial case (see Table III): The value of $\sin^2\theta'$ is 3/5, but largely irrelevant for cosmology since $T_{3R}^{\nu'} = 0$.

Coupling	Value	Comments
$\bar{\nu}'_R\gamma_\mu X_s^\mu t_R$	$\sqrt{k\pi R}\frac{g_4}{\sqrt{2}}a_{t_R\nu'_R}$	$a_{t_R\nu'_R} \sim \sqrt{a_{t_R}}$
$\bar{\nu}'_R\hat{\nu}'_R\phi$	$\frac{m_{\nu'_R}}{\Lambda_r}$	Same as in Table V

g_{LR} is unrelated to g_4), but a benchmark value for this mixing angle is 6/7.

(xi) We use an equivalence theorem so that $W/Z_{\rm long}$ is the unphysical Higgs.

(xii) Finally, the coupling of the ν' to the radion has an additional dependence on c for t_R only for the case $m_{\nu'} \lesssim M_{\rm KK}/\sqrt{k\pi R}$, which occurs for c for $t_R \lesssim -1/2$ (in the convention that $c = 1/2$ is a flat profile for t_R). Since we are most likely not interested in this DM mass region, no factor of a is shown here in the coupling of the DM to the radion.

IV. IMPLICATIONS FOR COSMOLOGY AND ASTROPHYSICS

The potentially light radion, an intrinsic ingredient of the model, has significant implications for cosmology and astrophysics. The existence of a light degree of freedom opens the possibility of an enhancement factor in the velocity-weighted annihilation cross section, relevant for the current epoch, compared to the cosmological value at freeze-out. This effect occurs via the SE [26]. An enhancement is required in order for annihilation signals to overcome astrophysical backgrounds, which would drown those signals for a TeV thermal relic with a canonical cross section $\langle\sigma v\rangle \sim$ few 10^{-26} cm^3 s^{-1}.

In Sec. IV A we explore the SE arising in our framework. Requiring a very large enhancement dictates special correlations between model parameters, as well as constrains the radion mass. In Sec. IV B we proceed to identify the parameter region compatible with direct detection limits and with the DM relic density implied by WMAP data. We find that a sizable SE factor is possible, and that the model consistent with full unification is viable over a large region of parameter space.

Indirect detection searches in Galactic cosmic rays, including high energy gamma rays and neutrinos as well as antiprotons, provide constraints on the viable magnitude of the SE factor. We study those limits in Secs. IV C 3 and IV C 4. For antiproton energies $\epsilon \gtrsim 10$ GeV, no detailed assumptions are required regarding the propagation in the Galaxy. We study possible imprints of our model in the high energy antiproton flux, accessible to existing and near future experiments. We find that in a sizable fraction of our parameter space (with heavy DM and a PGB radion), a $\bar{p}/p$ future signal is quite generic.

Regarding CR positrons, as discussed in the Introduction, an intriguing hint was reported by the PAMELA experiment, suggesting a spectral behavior which cannot be easily reconciled with simple diffusion models of CR propagation [1]. In our view, this latter observation does not necessitate an exotic injection mechanism for the positrons, and we dedicate Secs. IV C 5 to a discussion of this point. Here we comment that our benchmark models—which survive the requirements from direct detection, provide the correct DM relic density, and adhere to collider and precision test constraints—do not exhibit a large enough leptonic vs hadronic branching ratio as required to explain the positron fraction rise within the commonly adopted diffusion models.

A. Sommerfeld enhancement with a light radion

In this section we review the computation of the Sommerfeld enhancement factor, which is relevant for our framework if the radion is much lighter than the dark matter particle [26]. Requiring the maximal level of enhancement, SE $\gtrsim 10^4$, implies particular correlations between model parameters. We outline these correlations and show, in addition, that lower values of SE $\sim 10^2$–10^3 are easily accessible.

The Sommerfeld enhancement due to Yukawa interactions is found by solving the ordinary differential equation [23]

$$\left[\frac{d^2}{dx^2} + \frac{e^{-\epsilon_\phi x}}{x} + \epsilon_v^2\right]\chi(x) = 0, \tag{7}$$

with

$$\epsilon_v = \frac{v}{\alpha}, \qquad \epsilon_\phi = \frac{m_r}{\alpha M}, \qquad \alpha = \frac{\lambda^2}{4\pi} \tag{8}$$

and with the boundary conditions

$$\chi(x \to 0) \to 0, \qquad \chi(x \to \infty) \to \sin(\epsilon_v x + \delta). \tag{9}$$

Above, M is the mass of the annihilating particles, v is the velocity of each particle in the center of mass (CM) frame, λ is the Yukawa coupling, and m_r is the radion mass. The enhancement factor is then given by

$$\mathrm{SE} = \left|\frac{\frac{d\chi}{dx}(x \to 0)}{\epsilon_v}\right|^2. \tag{10}$$

Using (8) we find, for our model,

$$\lambda = \frac{M}{\Lambda_r}, \qquad \alpha = 7.9 \times 10^{-2}\left(\frac{M}{\Lambda_r}\right)^2,$$
$$\epsilon_v = 6.3 \times 10^{-3}\left(\frac{v}{150\ \mathrm{km\,s^{-1}}}\right)\left(\frac{M}{\Lambda_r}\right)^{-2}, \tag{11}$$
$$\epsilon_\phi = 1.2 \times 10^{-1}\left(\frac{m_r/M}{10^{-2}}\right)\left(\frac{M}{\Lambda_r}\right)^{-2}.$$

To get the effective enhancement one needs to average the SE over the DM velocity distribution, which we take as a Maxwell-Boltzmann distribution:

$$f(v) \propto v^2 e^{-v^2/2\sigma^2}, \tag{12}$$

where σ is the rms velocity, $\sigma = \sqrt{\int dv f(v) v^2/3}$. Here we use $\sigma = 150\ \mathrm{km\,s^{-1}}$ [66,67]. Uncertainties of $\mathcal{O}(1)$ associated with the value of the DM velocity distribution could modify some of the details of our results, notably, when a maximal level of enhancement is considered; yet they would not change the overall conclusions nor the detailed results in cases where only moderate enhancement levels of order SE $\sim 10^2$ are discussed.

The Sommerfeld factor attainable for our model is depicted in Fig. 2. In the left panel, the SE is plotted in the $(M/\Lambda_r, m_r/M)$ plane. Resonance branches cross the $(M/\Lambda_r, m_r/M)$ plane, with an enhancement factor SE $\gtrsim 10^4$ attainable at the peak of each branch and values of SE $\sim 10^3$ in the peak vicinity. The location of the ith resonance branch in the $(M/\Lambda_r, m_r/M)$ plane follows contours of constant values of $\epsilon_\phi = \epsilon_{\phi,i}$, with $\epsilon_{\phi,i} \approx 0.6, 0.15, 0.07, \ldots$ arising in the numerical solution of the Yukawa problem. Using Eq. (11) we see that the resonance branches correspond to parabolas,

$$\frac{m_r}{M} \approx C_i\left(\frac{M}{\Lambda_r}\right)^2, \tag{13}$$

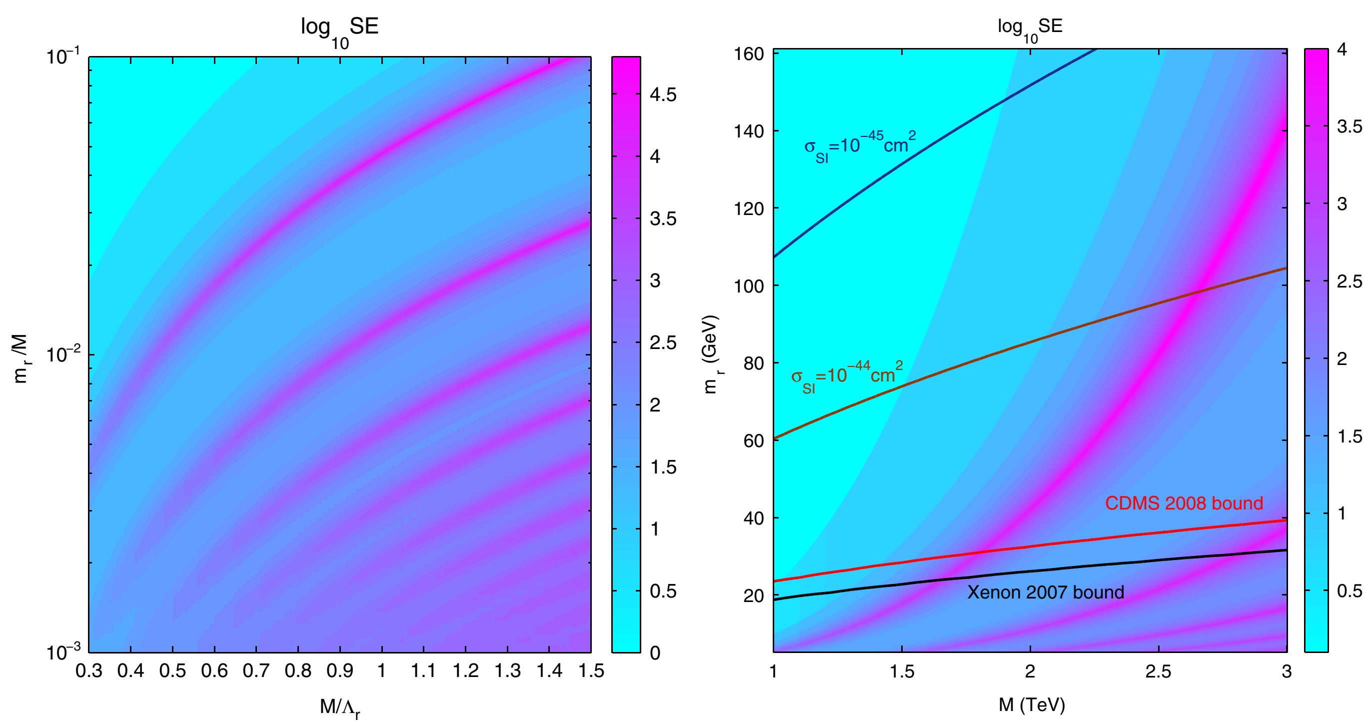

FIG. 2 (color online). Left panel: SE factor projected onto the $(m_r/M, M/\Lambda_r)$ plane; m_r, M, Λ_r stand for the radion mass, the dark matter mass, and the scale which suppresses the radion's couplings. Right panel: SE and direct detection bounds, projected onto the (m_r, M) plane at fixed $\Lambda_r = 3$ TeV.

where the C_i's are constant numbers. Sample values are $C_1 \approx 0.05$, $C_2 \approx 0.01$ for the first (upper) two resonance branches. We see that in order to obtain SE $> 10^3$, significant correlation is required between m_r, M, and Λ_r. Below we exploit this correlation to extract benchmark model points with interesting consequences for indirect signatures in Galactic cosmic rays. Note that the scenarios we consider require only moderate SE ~ 100, in order to yield observable CR signatures. As evident from Fig. 2, the parameter correlation can be relaxed in this case, and we use it primarily to delineate the relevant parameter region. The benchmark models we will consider can easily be located on the right panel of Fig. 2, in which we plot the SE in the (m_r, M) plane for a fixed value of $\Lambda_r = 3$ TeV. Direct detection constraints (discussed in the next section) are also superimposed on this panel.

Finally, note that the constraint discussed in Ref. [68] from correlation between Sommerfeld enhancement and relic density is *not* applicable in our case since the relevant particles involved in the two processes are different. Furthermore, since our force carrier, the radion, is not ultralight, higher partial waves beyond the s wave are negligible in the current epoch annihilation, and constraints due to enhanced DM self-scattering [68,69] are easily satisfied.

B. Dark matter relic density and direct detection limits

1. Relic density

As already anticipated the DM abundance is correlated with the DM-Z' coupling size, in particular, whether $T_{3R}^{\nu'}$ vanishes or not; we discuss the two cases separately in the following. The analytical expressions for the various annihilation cross sections can be found in [41]; here we only discuss the main qualitative feature of the model's parameter space. We compute the annihilation cross section using MicrOMEGAs 2.2 [70] for the numerical evaluation of the freeze-out DM abundance (for simplicity, we have set the KK Z-Z' mixing to zero [41,71]).

One important feature of our models is that our DM candidate mass, which is the RH top partner, is correlated with the localization of (or in 4D dual language, the amount of compositeness of) t_R, which in turn controls the relic density [41]:

$$m_{\mathrm{DM}}(c) \approx \begin{cases} 0.65(c+1)M_{\mathrm{KK}} & \text{if } c > -0.25 \\ 0.83\sqrt{c+\frac{1}{2}}M_{\mathrm{KK}} & \text{if } -0.25 > c > -0.5 \\ 0.83\sqrt{c^2-\frac{1}{4}}M_{\mathrm{KK}}\exp[k\pi R(c+\frac{1}{2})] & \text{if } c < -0.5, \end{cases} \tag{14}$$

where $M_{\mathrm{KK}} \approx 2.5\tilde{k}$ [with $\tilde{k} = k\exp(-k\pi R)$] is the leading order $(++)$ KK gauge boson mass and c stands for the t_R bulk mass. For instance, for $c > -1/4$ one finds $m_{\nu'} \approx \tilde{k}\pi(1+c)/2$ and for $-0.4 < c < -1/4$, $m_{\nu'} \approx 2\tilde{k}\sqrt{1/2+c}$.

In our calculations, we have neglected (for simplicity) the brane-localized kinetic term (BKT) for bulk fields. BKT's can, in principle, be used to control the total annihilation cross section and direct detection rate as follows [72]. First, BKT's for gauge fields tend to lower the coupling of the lightest gauge KK modes to other particles localized near the TeV brane. Such BKT's also lower the gauge KK mass relative to the going rate, $\tilde{k}$, mentioned above. However, electroweak precision tests (in particular, the S parameter) put a lower bound of a few TeV on the lightest KK scale which is (roughly) independent of the coupling of this KK mode. Combining these two features, we see that the annihilation cross section, and similarly direct detection, can be reduced by BKT's for gauge fields. However, $\tilde{k}$ is then larger than a few TeV which might introduce a severe little hierarchy problem into the model. In addition, BKT's for fermions can modify the correlation between DM mass and localization of t_R and, in turn, some of our conclusions.

We find that DM annihilation into two radions requires the DM pair (fermion-antifermion) to be in a p wave, and hence is suppressed (see also Ref. [33]).[19] Thus this channel is not relevant for the calculation of relic density, nor does it get SE.

Nonvanishing DM-Z' coupling.—For $T_{3R}^{\nu'} \neq 0$, we find, quite generally, that there is tension between obtaining the correct relic density and being consistent with bounds from direct detection. This is associated with the large $\nu'\bar{\nu}'Z'$ coupling, which is enhanced relative to the SM gauge couplings by the RS volume factor, $\sqrt{k\pi R} \sim 6$ (or, as expected, via the AdS/CFT correspondence, which is an intercomposite coupling).[20] Furthermore, the large $T_{3R}^{\nu'}$ $(=2)$

[19] In general, if the interactions respect parity, then only p-wave annihilation of the fermion-antifermion into a pair of identical scalars is allowed [73].

[20] A smaller volume factor would thus result in suppression of the DM annihilation and direct detection rates. For example, since the focus here is on unification, one can assume that the UV brane scale is actually the unification scale, instead of the canonical choice of Planck scale which gives $\sqrt{k\pi R} \sim 6$. However, we have verified that, since the unification scale is only 2 orders of magnitude below the Planck scale, the resulting improvement is only incremental. Hence the conclusion about the viability of these models is basically unchanged. One can, in principle, consider a *much* smaller RS volume [42,74]. However, then the SM level of unification of gauge couplings, and hence the motivation for considering a GUT model (and, in turn, the above DM candidate), is lost.

for **10** of $SU(4)$ and the fact that $\cos^2\theta'$ is significantly smaller than 1 (see Table V), $\cos^2\theta'_{\mathbf{35}} \sim \frac{1}{7}$, for a model with **35** of $SU(4)$ make the rates even larger. Depending on the mass of ν' compared to the intermediate particle, $\nu'\bar{\nu}'$ annihilate into the SM particles dominantly through either s-channel (for $2M_{\nu'} \leq M_{Z'}$) or t-channel (for $2M_{\nu'} > M_{Z'}$) annihilation. We find that in the former case the Z' becomes broad enough such that resonance enhancement of the cross section strongly suppresses the relic abundance, for $M_{Z'} \sim 2M_{\nu'}$. For $M_{\nu'} \ll M_{Z'}$ the off-resonance cross section is suppressed by $M_{\nu'}^2/M_{Z'}^2$. Hence, for $M_{\nu'} \lesssim M_{Z'}/5$ the resulting density is in the right ballpark. The case with more massive DM, $2M_{\nu'} > M_{Z'}$, has no kinematical suppression factors and yields a negligible freeze-out density.

We show in Fig. 3 the resulting $\Omega_{\rm DM}h^2$ for partially unified models [$\nu' \in \mathbf{10}$ as in Table VIII (**35** in Table II)] as a function of the DM mass. Curves are shown for $M_{\rm KK} = 3$, 4 TeV, where the green curve indicates the corresponding relic density due only to annihilation into the EW sector, which is rather robust, while the blue curve shows how the density is further suppressed when the coupling of Z' to the top quark pair is added (we used the canonical choice of $\sin\theta'$ given by setting $g_{LR} = g_4$, which is less robust). The annihilation rate is calculated assuming the mass relation of Eq. (14), and the smallest possible coupling $g_{LR} = 0.35$. This choice of g_{LR} minimizes the rate; i.e., the resulting relic densities can be made much smaller by allowing larger g_{LR}, but not much larger (which, as we will show below, induces a strong constraint on these models). Other parameters were not varied. For concreteness, we used $M_{Z'} = M_{\rm KK}$, $\Lambda_r = M_{\rm KK}$, and $T_{3R}^{\nu'} = 1$ for relic density calculation.

TABLE VIII. Another model with custodial representations for b_L and RH leptons and with nonvanishing $\nu'\bar{\nu}'Z'$ coupling: The subscripts denote the $\sqrt{8/3}\, X$ charge.

	$SU(4)_c \sim SU(3)_C \times U(1)_X$	$SU(2)_L$	$SU(2)_R$
t_R, ν'	$\mathbf{10} \sim \mathbf{3}_{2/3}, \mathbf{1}_2 \ldots$	**1**	**5**
$(t, b)_L$	$\mathbf{10} \sim \mathbf{3}_{2/3}, \ldots$	**2**	**4**
τ_R	$\bar{4} \sim \mathbf{1}_{-1}, \ldots$	**1**	**1**
$(\nu, \tau)_L$	$\bar{4} \sim \mathbf{1}_{-1}, \ldots$	**2**	**2**
b_R	$\mathbf{10} \sim \mathbf{3}_{2/3}, \ldots$	**1**	**5**
H	**1**	**2**	**2**

For the model with **10** of $SU(4)$, for $M_{\rm KK} = 4$ TeV, we see that there is a sizable region of DM mass, i.e., below 600 GeV, which gives the correct relic density. On the other hand, only the small region below 200 GeV works for a model with **35** of $SU(4)$. However, as discussed in the following, typically both these regions imply a too-large rate for the direct detection experiments.

Vanishing DM-Z' coupling.—In this case, since DM coupling to Z' vanishes, the dominant annihilation channel is via t-channel X_s exchange into final state heavy quarks, say $t_R\bar{t}_R$ (see Table VI). As mentioned, the rate is controlled by the amount of compositeness of the RH tops, which is also correlated (modulo BKT's for fermions) with the DM mass as in Eq. (14). Thus, within this case, an interesting correlation between the DM mass and the re-

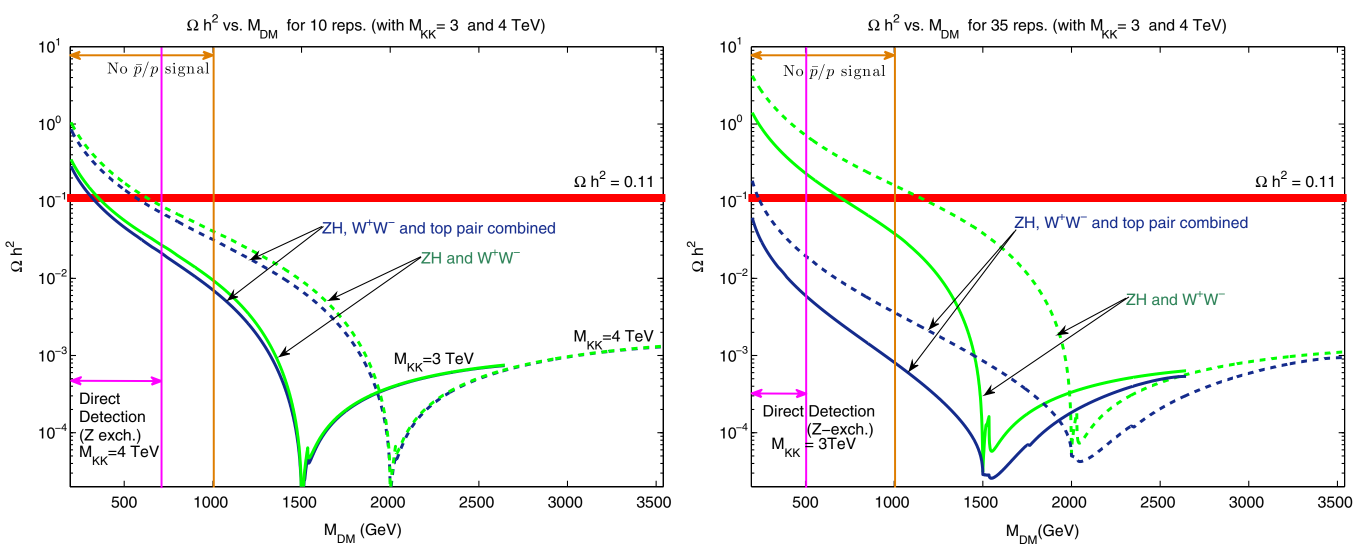

FIG. 3 (color online). Relic density Ωh^2 vs the DM mass for the partially unified models with $\nu' \in \mathbf{10}\,(\mathbf{35})$ on the left-hand side (right-hand side). Solid curves correspond to $M_{\rm KK} = 3$ TeV and dashed ones to $M_{\rm KK} = 4$ TeV and $g_{LR} = g_4 = 0.35$. Also shown, as vertical lines, are the constraints from direct detection (purple, leftmost vertical line) and the region (gold) where typically no future $\bar{p}/p$ can be observed. A direct detection bound for $M_{\rm KK} = 3$ TeV with **10** of $SU(4)$ is not shown because, for this case, the entire range of DM mass considered here is ruled out by the central value of the direct detection bound, while $M_{\rm KK} = 4$ TeV with **35** of $SU(4)$ is not shown because, in that case, the central value is ~40 GeV, which is below the smallest DM mass shown in the plot; i.e., direct detection is a weak constraint in this case.

sulting relic abundance is obtained. This is also interesting in the context of precision GUT, which probably requires a composite RH top [46]; however, the issue of precision custodial unification is beyond the scope of this project. We show in Fig. 4 the resulting $\Omega_{\rm DM}h^2$ for the simplest fully unifiable model as a function of the DM mass. Bands for $M_{Z'} = 3$ and 4 TeV are shown, obtained by scanning g_{LR} over the favored range $g_{LR} = 0.35 - 1$ while keeping other parameters fixed. We see that there is a significantly larger region of the parameter space (than in the previous models), i.e., a few 100 GeV to a few TeV, which yields the correct DM abundance. This feature is due mainly to the absence of Z' exchange in the simplest fully unifiable model. However, the more important impact of the absence of DM coupling to Z' is that this model is easily consistent with bounds from direct detection experiments (cf. other two models).

2. Direct detection limits

Many experiments are underway currently to directly detect dark matter, and still more are proposed to improve the sensitivity. In order to ascertain the prospects of directly observing ν' in the model framework we are considering, we compute the elastic ν'-nucleon cross section due to the t-channel exchange of the radion, which is the most important channel, when the radion mass is very light. The other important channel is t-channel exchange of the Z, which was computed in [41,75].

While contributions from radion exchange are generic within our framework, the ones induced by Z exchange (via Z-Z' or via ν_R'-KK ν_L^c mixing) only occur in the partially unified model and not in the simplest fully unifiable model (where the ν' coupling is custodially protected).

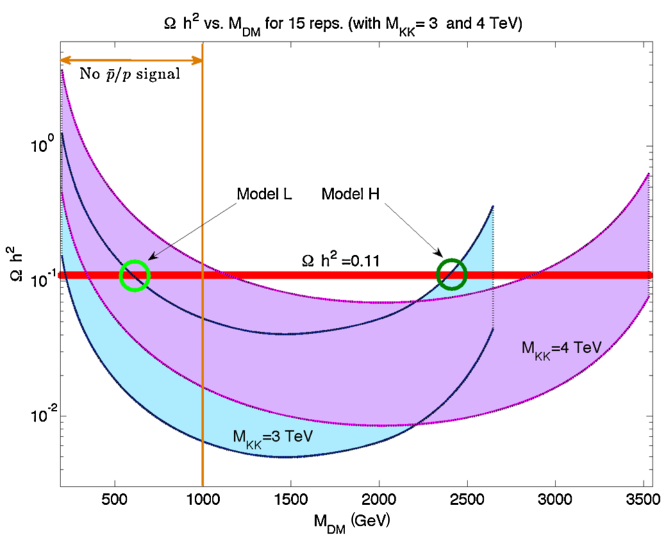

FIG. 4 (color online). Relic density Ωh^2 vs the DM mass for the simplest fully unifiable model with $\nu' \in \mathbf{15}$. The bands correspond to varying the coupling in the favored range $g_{LR} = 0.35$–1 and $M_{\rm KK} = 3$, 4 TeV. The points relevant to our two benchmark models ("model L" and "model H") are shown as the two light and dark green circles, respectively.

The cross section for Z exchange is (roughly) independent of DM mass, but scales as $M_{\rm KK}^{-4}$. However, the CDMS bound scales as $1/M_{\rm DM}$ (i.e., inverse of the number density of DM) and hence becomes dominant at low masses and tightly constrains the light DM region as shown by the (leftmost) purple vertical lines of Fig. 3. Several astrophysical unknowns (such as the local DM profile, the velocity distribution, etc.) are involved in converting the direct detection bound into a constraint on a microscopical model parameter space (see e.g. [76]). Nevertheless, for concreteness, taking central values seriously, only a very small region survives for $M_{\rm KK} = 4$ TeV (none for $M_{\rm KK} = 3$ TeV) for **35** of $SU(4)$, and none for **10** of $SU(4)$. Note that the direct detection bound for $M_{\rm KK} = 3$ TeV with **10** of $SU(4)$ is not shown because for this case the entire range of DM mass considered here is ruled out by the central value of the bound. For $M_{\rm KK} = 4$ TeV with **35** of $SU(4)$ the bound is not shown because in that case the central value (DM mass ~40 GeV) is below the smallest mass shown in the plot (i.e., effectively the direct detection bound is weak in this case so that the relic density constraint is more important). The reason why the model with DM in **10** of $SU(4)$ turns out to be more constrained by direct detection than the model with **35** of $SU(4)$ is due to the fact that $T_{3R}^{\nu'}$ in the former model is twice as large as in the latter model, while the θ' dependence of the effective DM coupling to Z (which controls the interaction with the nuclei) cancels (see Table V). We do not include the contribution to direct detection from the radion exchange here since it is highly model dependent, and can be easily made subdominant for a suitable choice of radion mass and Λ_r.

However, as mentioned already, DM coupling to Z' vanishes for the simplest unified model of **15** of $SU(4)$, which means that t-channel exchange of Z also becomes irrelevant for direct detection bounds. Hence, for this model, t-channel exchange of the radion is the single most important channel, and direct detection bounds can give information for Λ_r and radion mass. In the CM frame, in the nonrelativistic limit, the elastic cross section for radion exchange is approximately given as

$$\sigma(\nu' N \to \nu' N) \approx \frac{M_{\nu'}^2 \lambda_N^2}{4\pi v_{\rm rel} \Lambda_r^2} \frac{(|\mathbf{p}_{\nu'}|^2 + m_N^2)}{(t - m_r^2)^2}, \qquad (15)$$

where $|\mathbf{p}'_\nu| \approx M_{\nu'} v_{\nu'}$, $v_{\nu'} \sim 10^{-3}$ is the DM velocity in the CM frame, $m_N \approx 1$ GeV is the nucleon mass, $\lambda_N/\sqrt{2}$ is the effective $r\bar{N}N$ coupling, and t is the Mandelstam variable, which can be ignored compared with m_r^2 in the radion propagator. For the radion-nucleon coupling we find the typical magnitude $\lambda_N \sim 10^{-6}$, which includes the radion tree-level coupling to light quarks (u, d, s) and gluons, and the heavy-quark-loop two-gluon couplings, with the leading parametric dependence $\lambda_N \propto m_N/\Lambda_r$. A subleading dependence on the mass of the radion arises because the radion couplings to gauge boson pairs depend on m_r. All in all, the model parameters enter the direct detection computation in the following way:

$$\sigma(\nu' N \to \nu' N) \propto \frac{M_{\nu'}^2 m_N^4}{\Lambda_r^4 m_r^4}. \tag{16}$$

For heavy DM, one factor of m_N^2 should be replaced by a factor of $M_{\nu'}^2$ arising from the large momentum carried by the heavy ν_R' and entering the numerator of (15). Finally, note that while Eq. (15) provides a reasonable approximation, useful for obtaining an analytical understanding of the parameter dependencies of the direct detection constraints, in practice we incorporate our model into the MicrOMEGAs [70,77] package and compute the direct detection bound numerically. We find that the numerical results follow the parametric dependence given in Eq. (16) rather well.

Our results are illustrated in Fig. 2, where the direct detection constraints are superimposed on top of the SE factor. Taking the direct detection limits at face value, we find that a very light radion of $m_r \lesssim 20$ GeV is already excluded by both the CDMS and Xenon experiments. The CDMS limit disfavors m_r of up to $\sim$40 GeV for a DM mass as high as 3 TeV. The entire region of the remaining parameter space, where our analysis is valid, will be probed by upcoming experiments, such as SuperCDMS and Xenon 1-ton [78].

C. Indirect detection: Simplest fully unifiable model

In the following sections we evaluate the implications of our framework to various CR species. As we have discussed above, models where the DM is not custodially protected are in tension with direct detection experiments or lead to too-low relic density. We therefore focus on the unifiable model where the DM-Z' coupling vanishes. To facilitate the discussion we introduce two benchmark models and study the resulting CR injection spectra and rates. We then move on to signatures in photons and neutrinos. High energy photon and neutrino observations constrain the DM annihilation cross section, weighted by the integral of the DM number density–squared along the line of sight of the experiment.

Proceeding to antiprotons, we note that the astrophysical background is constrained by existing CR data. Subject to a few general assumptions, the effect of propagation in the Galaxy can be accounted for at the cost of introducing a single additional fuzz factor. The antiproton analysis is, in this sense, as predictive as the analysis of photon signals where the analogous fuzz factor is contained in the line-of-sight integral. Lastly, we turn to the more involved case of positron signals and briefly discuss the injection rate of $e^+/\bar{p}$, for which the astrophysical background is somewhat easier to interpret.

1. Benchmark models and CR injection spectrum

Following the discussion of the relic density, Sommerfeld enhancement, and direct detection bounds, we focus here on two viable benchmark model points characterized by different values of DM and radion masses which result, in turn, in different annihilation spectra. We keep fixed the value of the Z' mass, $m_{Z'} = 3$ TeV. The benchmark models are defined as follows.

Model L.—$M = 600$ GeV, $m_r > 40$ GeV, which corresponds to the LH circle on Fig. 4. In principle, one can obtain a sizable SE while decreasing Λ_R; however, in this case we find tension with direct detection bounds (from radion exchange).

Model H.—$M = 2400$ GeV, $m_r = \mathcal{O}(100)$ GeV, which corresponds to the RH circle on Fig. 4. In this case there is a wide range of radion masses and corresponding Λ_R which yield a sizable SE, consistent with direct detection experiments.

In both cases the annihilation is dominated by $\bar{\nu}'\nu' \to t_R \bar{t}_R$ via t-channel X_s exchange. The couplings are given in Table VI, while Eq. (14) links the top compositeness with the DM mass.

The CR injection spectra of stable final states are plotted in Fig. 5 for the various benchmark points. These spectra, together with the DM mass and Sommerfeld enhancement factor, serve as the particle physics input required for the calculation of indirect detection signals.

2. CR production rate

The production rate of a cosmic ray species α due to annihilation of Dirac fermion DM at a given spatial position $\vec{r}$ in the Galaxy is given by

$$Q_{\alpha,\mathrm{DM}}(E, \vec{r}) = \frac{1}{4} n^2(\vec{r}) \frac{d\sigma v(\mathrm{DMDM} \to \alpha)}{dE}. \tag{17}$$

Here $n(\vec{r})$ is the total DM number density (particle + antiparticle) and $\frac{d\sigma v(\mathrm{DMDM}\to\alpha)}{dE}$ is the differential velocity-weighted annihilation cross section for the production of the species α. It is convenient to work with dimensionless quantities,

$$\epsilon = \frac{E}{\mathrm{GeV}}, \qquad M_1 = \frac{M}{\mathrm{TeV}},$$
$$\overline{\sigma v} = \frac{\sigma v}{6 \times 10^{-26}\ \mathrm{cm}^3\,\mathrm{s}^{-1}}, \qquad n_o(\vec{r}) = \frac{n(\vec{r})}{n(\vec{r}_{\mathrm{sol}})}, \tag{18}$$

where M is the DM mass, σv is the total velocity-weighted annihilation cross section, $\vec{r}_{\mathrm{sol}} \approx 8.5$ kpc is the distance between the solar system and the Galactic center, and $n(\vec{r}_{\mathrm{sol}}) = 0.3\ \mathrm{cm}^{-3}\,\mathrm{GeV}/M$ is the DM number density in the local halo. For the local halo mass density, we adopt a value of $\rho_{\mathrm{DM}}(\vec{r}_{\mathrm{sol}}) = 0.3\ \mathrm{GeV\,cm}^{-3}$. Order-one deviations for this number are possible, both on average and due to local clumps, and go through to the computed CR flux. With the definitions (18), the CR production rate can be

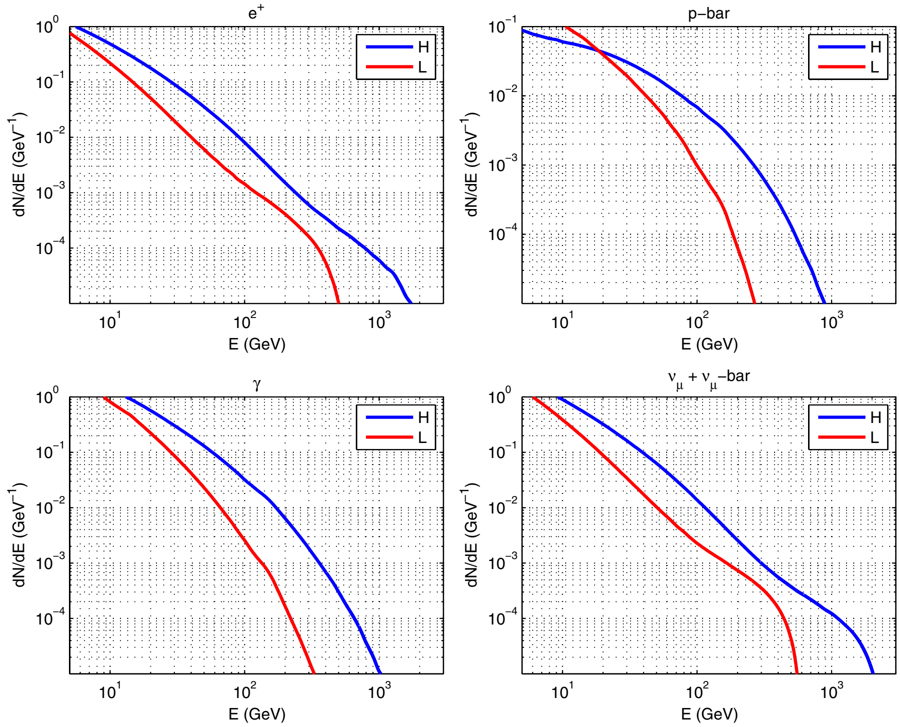

FIG. 5 (color online). Decayed final state annihilation spectra for the two benchmark models.

written as

$$Q_{\alpha,\mathrm{DM}}(\epsilon, \vec{r}) = Q_{\alpha,\mathrm{DM}}(\epsilon, \vec{r}_{\mathrm{sol}}) \times n_o^2(\vec{r}), \tag{19}$$

with the local injection rate

$$Q_{\alpha,\mathrm{DM}}(\epsilon, \vec{r}_{\mathrm{sol}}) = 1.3 \times 10^{-33} \frac{\overline{\sigma v}}{M_1^2} \frac{dN_\alpha}{d\epsilon} \ \mathrm{cm}^{-3}\,\mathrm{s}^{-1}\,\mathrm{GeV}^{-1}, \tag{20}$$

and where $\frac{dN_\alpha}{d\epsilon}$ is the differential number of stable final state particles of species α emitted per annihilation event. In writing Eq. (19) we have neglected the spatial dependence in the Sommerfeld enhancement [79]. As, in this paper, we do not attempt to provide a detailed description of the spatial features of the DM annihilation signal, we neglect this possible complication throughout the discussion.

The rate of DM annihilation is proportional to the number density squared, and so the results, in particular as concerns photon and neutrino flux from the Galactic center region, depend on the assumed profile. The latest N-body simulations, including only DM and no baryons, point to DM halo profiles with a cusped central region. However, the inner zone of a few hundred parsecs from the center remains uncertain. In addition, the effect of baryons may be significant at the central region, and its impact on the DM distribution is far from understood. Baryons were argued to either increase the inner cusp, or actually smooth it out, resulting in a cored profile [80,81]. In this work we analyze both cusped and cored DM halo profiles. The examples we consider are the cusped NFW [82] and the cored isothermal sphere [83] (denoted below by ISO). We do not attach special significance to any particular profile but rather lay out the consequences of each case regarding indirect detection prospects for our framework. The radial dependence of the halo distributions is

$$\text{NFW:}\quad \frac{\rho(r)}{\rho(r_{\mathrm{sol}})} = \frac{r_{\mathrm{sol}}}{r}\left(\frac{1 + r_{\mathrm{sol}}/r_s}{1 + r/r_s}\right)^2, \qquad r_s = 20\ \mathrm{kpc},$$
$$\text{ISO:}\quad \frac{\rho(r)}{\rho(r_{\mathrm{sol}})} = \frac{1 + r_{\mathrm{sol}}^2/r_s^2}{1 + r^2/r_s^2}, \qquad r_s = 5\ \mathrm{kpc}. \tag{21}$$

3. Photons and neutrinos

The incoming flux of photons or neutrinos per unit solid angle is obtained by integrating the production rate along the line of sight in a given direction Ω in the sky,

$$j(\Omega, \epsilon)d\Omega = d\Omega \int_{\mathrm{l.o.s.}} dr r^2 \frac{Q_{\gamma(\nu),\mathrm{DM}}(\epsilon, \vec{r})}{4\pi r^2}$$
$$= Q_{\gamma(\nu),\mathrm{DM}}(\epsilon, \vec{r}_{\mathrm{sol}}) \times \frac{d\Omega}{4\pi} \int_{\mathrm{l.o.s.}} dr n_o^2(\vec{r}). \tag{22}$$

Gamma-ray observatories report limits on $\bar{j}(\Omega, \epsilon)$, defined by averaging (22) over the acceptance $\Delta\Omega$ of the experiment,

$$\bar{j}(\Omega, \epsilon) = \frac{1}{\Delta\Omega} \int_{\Delta\Omega} d\Omega\, j(\Omega, \epsilon). \tag{23}$$

The observed photon flux depends on the local injection rate, up to a single overall model-dependent factor given by the line-of-sight integral, which encodes the DM distribution.

We derive gamma-ray-based model constraints from the following data sets, provided by the HESS imaging air Cherenkov detector.

(i) HESS observations of the Galactic center (GC) [84]: The GC data set corresponds to the inner 0.1° of the GC gamma-ray source, HESS J1745-290. The energy range was $E_\gamma > 160$ GeV. Considering the uncertainties involved in the calculation, we find it sufficient for our purpose to use the power-law fit reported by the HESS Collaboration, $\bar{j} \propto E^{-\Gamma}$, with $\Gamma = 2.25 \pm 0.04(\mathrm{stat}) \pm 0.10(\mathrm{syst})$. The normalization is defined from the reported value of the integrated flux above 1 TeV, $\int_{1\,\mathrm{TeV}} dE \bar{j} \Delta\Omega = [1.87 \pm 0.10(\mathrm{stat}) \pm 0.30(\mathrm{syst})] \times 10^{-12}\,\mathrm{cm}^{-2}\,\mathrm{s}^{-1}$. For definiteness, we use the central values for the reported flux and impose that the photon flux resulting from DM annihilation does not exceed it in order to derive constraints on the model.

(ii) HESS observations of the Galactic ridge area (GR) [85]: The GR data set corresponds to an observation of the rectangular angular patch $|l| < 0.8°$, $|b| < 0.3°$, from which the spectral components of the sources HESS J1745-290 and G0.9 + 0.1[21] were subtracted. The energy range was $E_\gamma > 170$ GeV. We use the power-law fit reported by the HESS Collaboration, $\bar{j} = k(\frac{E}{\mathrm{TeV}})^{-\Gamma}$, with $\Gamma = 2.29 \pm 0.07(\mathrm{stat}) \pm 0.20(\mathrm{syst})$ and the normalization $k = [1.73 \pm 0.13(\mathrm{stat}) \pm 0.35(\mathrm{syst})] \times 10^{-8}\,\mathrm{TeV}^{-1}\,\mathrm{cm}^{-2}\,\mathrm{s}^{-1}\,\mathrm{sr}^{-1}$. We use the central values for the reported flux and impose that the photon flux resulting from DM annihilation does not exceed it in order to derive constraints on the model.

Data from the Fermi-LAT satellite-borne detector have recently become available. We analyzed the preliminary results presented in [87] for the Galactic center region. These data constrain the lower energy part of the spectrum and, for model L with a cuspy DM profile, is competitive with the HESS data.

The situation is illustrated in Fig. 6, in which we plot the GC data set of Fermi and HESS vs model signals, evaluated with an NFW DM halo profile and the maximal Sommerfeld factor allowed by the GC data set. (Note that, for model H, the HESS GR data set is in fact more constraining, and a value of SE = 180, used in the figure for illustration, is excluded.)

Limits on the neutrino flux arise from measurements of the neutrino-induced muon flux in neutrino detectors. For DM mass M, the flux of muons at the detector is given by

$$\phi_\mu = \int_{\epsilon_{\mathrm{th}}}^{M} d\epsilon_\mu \int_{\epsilon_\mu}^{M} d\epsilon_\nu \bar{n}_N \bar{j}_{\nu_\mu}(\Omega, \epsilon)\Delta\Omega \left[\frac{d\sigma^{\nu N}}{d\epsilon_\mu} + \frac{d\sigma^{\bar{\nu} N}}{d\epsilon_\mu}\right] L(\epsilon_\mu, \epsilon_t h). \tag{24}$$

[21] See [86] for the details of the source G0.9 + 0.1.

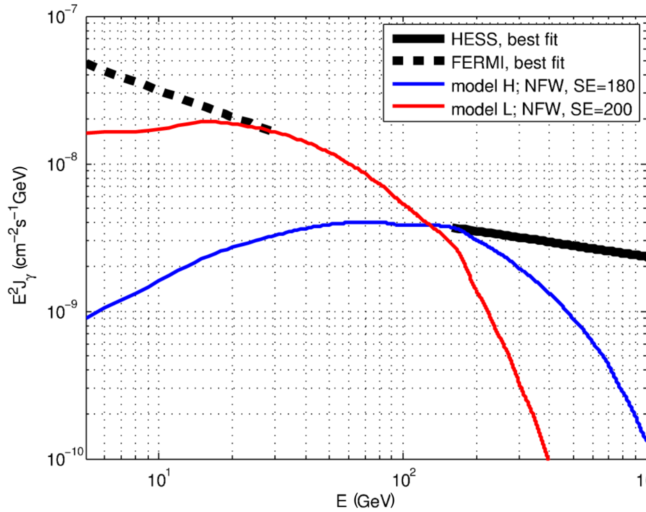

FIG. 6 (color online). Gamma-ray constraints from Fermi and HESS.

Here $j_{\nu_\mu}(\Omega, \epsilon)$ is the muon-neutrino flux at the Earth, which equals the antineutrino flux in the case of DM annihilation and is obtained from Eq. (23) (we use tribimaximal neutrino mixing for definiteness). The differential cross sections are given by

$$\frac{d\sigma^{\nu N}}{d\epsilon_\mu} = \frac{2G_F^2 \bar{m}_N}{\pi}\left[a_1 + a_2\left(\frac{\epsilon_\mu}{\epsilon_\nu}\right)^2\right], \tag{25}$$

with $a_1 \approx 0.2$, $a_2 \approx 0.05$ for neutrino-nucleon CC scattering and the same with $a_{1,2}$ interchanged for the antineutrino-nucleon case. The muon range in the rock beneath the detector is

$$L(\epsilon_\mu, \epsilon_{\mathrm{th}}) = \frac{1}{\rho\beta_\mu}\ln\left(\frac{\alpha_\mu + \beta_\mu\epsilon_\mu}{\alpha_\mu + \beta_\mu\epsilon_{\mathrm{th}}}\right), \tag{26}$$

where $\epsilon_{\mathrm{th}} = 1.6\,\mathrm{GeV}$ is the threshold energy for detection, and $\alpha_\mu \approx 2\times 10^{-3}\,\mathrm{GeV}\,\mathrm{cm}^2\,\mathrm{g}^{-1}$ and $\beta_\mu \approx 3\times 10^{-6}\,\mathrm{cm}^2\,\mathrm{g}^{-1}$ are the muon energy-loss coefficients. For the target material we consider a nucleon mass $\bar{m}_N = m_p$, and the nucleon number density is given by $\bar{n}_N = \rho/\bar{m}_N$.

We derive neutrino-based model constraints from the upper limits on the upward through-going muon flux, measured at Super-Kamiokande (SK) [88]. We use the 95% C.L. limits quoted in [89], where the line-of-sight integrals were also given for angular acceptances of 3°–30° and various DM halo profiles.

In Table VII we summarize the photon and neutrino constraints. Regarding observations of the Galactic center region, the line-of-sight integral depends on the assumed DM halo profile as well as the angular resolution of the experiment. Small changes in the halo profile around the poorly known central regions of the Galaxy result in significant variations in the predicted flux [92]. For the cored profile, large cancellations can occur due to background subtraction, and the resulting bound becomes weak [89] in comparison with antiproton and neutrino constraints. In

TABLE VII. Upper bounds on the Sommerfeld enhancement factor, resulting from HESS and Fermi γ and SK ν constraints. Square brackets refer to optimal background subtraction with the HESS resolution. For ν we report the result corresponding to the most constraining opening angle for the SK analysis. In case the bounds are weaker than 10^4, we keep only the order of magnitude. We also quote the analyses of Fermi constraints, provided in [90,91]; see text for details.

	GC, HESS γ [84]	GR, HESS γ [85]	GC, Fermi γ [87]	Fermi γ [90,91]	SK ν [88]
	NFW–ISO	NFW–ISO	NFW–ISO	NFW–ISO	NFW–ISO
L	260–[10^5]	310–[10^4]	200–10^7	50–500	4×10^3–10^4
H	180–[10^5]	130–[10^4]	900–10^8	100–10^3	5×10^3–10^4

this case, for the HESS analysis we report the bound without accounting for these cancellations (given inside square brackets in Table VII), such that the optimal performance can be assessed.

Coming back to the Fermi data, we note that part of the power of these measurements lies in the complete coverage of the sky. As a result, strong constraints can be derived also for cored DM profiles, which were effectively unconstrained by earlier measurements. A more complete treatment of the new Fermi data, which included the same final state annihilation products as in our model, was very recently provided in [90,91]. The analysis of these references is in good agreement with ours for observations of the Galactic center, but as expected, it presents much stronger bounds for the cored profile. In particular, according to [90,91], the SE for our model L(H) cannot exceed $\sim 500(10^3)$ in the ISO profile scenario. For an NFW profile, the SE for model L(H) is limited below $\sim 50(100)$.

Putting this all together and including the results of [90,91], we find that the neutrino bounds are subdominant in comparison with the new photon data, for any DM profile. Finally, note that with a realistic treatment of the backgrounds, the bounds we apply are likely to tighten by a factor of at least a few, implying that the SE factor for our models will probably be limited to a few tens (hundred) in the case where a cusped (cored) DM profile is adopted. As we show below, such a value of the SE is still sufficient to produce interesting antiproton signatures.

4. Antiprotons

The PAMELA experiment has recently measured the antiproton to proton flux ratio [6]. The reported antiproton fraction does not show deviations from the expected result, based on secondary production by pp and spallation interactions of primary CRs with an interstellar medium (ISM). Nevertheless, DM annihilation can contribute a primary component to the CR antiproton flux, with a production rate density given by Eq. (19). This contribution must be small at the currently explored energies, but could, in principle, reveal a peak at $\gtrsim 100$ GeV energies, soon to be measured by the PAMELA and (hopefully) AMS02 [30] experiments.

Cosmic ray antiprotons have long been considered as a good channel to detect exotic sources (see e.g. [93]). At high energies ($E > 10$ GeV) the background can be determined from the CR nuclei data [15,94,95], leaving significant predictive power.[22] As concerns the DM contribution, analyses in the literature were based on detailed propagation models. Such propagation models typically include additional free parameters which reduce the predictive power of the analysis. Here we show that the antiproton flux can be computed in a model-independent manner, at the cost of introducing one free parameter to the calculation. This parameter is an energy-independent effective volume factor, encoding the different spatial extensions of the DM and the spallation sources. The fact that only one free parameter is introduced makes the antiproton channel as predictive as the photon and neutrino channels, for which propagation in the Galaxy is trivial.

The approach we adopt is based on the fact that high energy antiprotons above a few GeV suffer only small energy losses as they travel through the Galaxy, and on the fact that the secondary antiproton flux up to $E\sim 300$ GeV can be computed in a model-independent manner, based on the existing CR nuclei data [15,94,95]. To proceed, we need the following ingredients.

The first ingredient concerns the propagation in the Galaxy. Define the quantity $G(\epsilon, \epsilon_S; \vec{r}, \vec{r}_S)$, encoding the propagation of CR antiprotons in the Galaxy, as follows:

$$n_{\bar{p}}(\epsilon, \vec{r}) = \int d^3 r_S \int d\epsilon_S Q_{\bar{p}}(\epsilon_S, \vec{r}_S) G(\epsilon, \epsilon_S; \vec{r}, \vec{r}_S), \quad (27)$$

where $Q_{\bar{p}}(\epsilon_S, \vec{r}_S)$ is the injection rate density at energy ϵ_S at the point $\vec{r}_S$, the spatial integral contains the confinement volume of Galactic CRs, and $n_{\bar{p}}(\epsilon, \vec{r})$ is the antiproton density at some point $\vec{r}$ in the Galaxy.[23] The negligible energy change of antiprotons above 10 GeV implies that $G(\epsilon, \epsilon_S; \vec{r}, \vec{r}_S) \propto \delta(\epsilon - \epsilon_S)$. We now make the assumption that G is separable, i.e. that

[22] In principle, CR antideuterons could also serve as good probes for exotic contributions [48]. However, available and upcoming data are limited to low energies $E \lesssim 3$ GeV/nuc, where propagation uncertainties render a model-independent analysis challenging.

[23] For simplicity, we did not introduce a time label in Eq. (27), which could account for deviations from a steady state. Provided that the explicit assumptions we make hold, adding time dependence to the problem would not change our basic result.

$$G(\epsilon, \epsilon_S; \vec{r}, \vec{r}_S) = \delta(\epsilon - \epsilon_S) g(\epsilon) \bar{G}(\vec{r}, \vec{r}_S). \tag{28}$$

The second ingredient concerns the secondary source spectrum. We assume that the injection spectrum (not rate) of secondary antiprotons has a homogeneous distribution in the Galaxy. In practice, this assumption amounts to demanding that spatial variations in the spectrum of primary CRs are small, at least in the regions from which most of the secondary antiprotons observed locally are generated. Under this assumption the secondary source term is separable,

$$Q_{\bar{p},\mathrm{sec}}(\epsilon, \vec{r}) = Q_{\bar{p},\mathrm{sec}}(\epsilon, \vec{r}_{\mathrm{sol}}) \times q_{\mathrm{sec}}(\vec{r}), \tag{29}$$

where $Q_{\bar{p},\mathrm{sec}}(\epsilon, \vec{r}_{\mathrm{sol}})$ is the local secondary injection rate.

Under the above assumptions, the local density ratio between the primary and secondary components takes the form

$$\frac{n_{\bar{p},\mathrm{DM}}(\epsilon, \vec{r}_{\mathrm{sol}})}{n_{\bar{p},\mathrm{sec}}(\epsilon, \vec{r}_{\mathrm{sol}})} = f_V \frac{Q_{\bar{p},\mathrm{DM}}(\epsilon, \vec{r}_{\mathrm{sol}})}{Q_{\bar{p},\mathrm{sec}}(\epsilon, \vec{r}_{\mathrm{sol}})}, \tag{30}$$

with the energy-independent volume factor

$$f_V = \frac{\int d^3 r q_{\mathrm{DM}}(\vec{r}) \bar{G}(\vec{r}_{\mathrm{sol}}, \vec{r})}{\int d^3 r q_{\mathrm{sec}}(\vec{r}) \bar{G}(\vec{r}_{\mathrm{sol}}, \vec{r})}. \tag{31}$$

For a DM annihilation source, we have $q_{\mathrm{DM}}(\vec{r}) = n_o^2(\vec{r})$. We can write the antiproton to proton flux ratio as follows,

$$\frac{J_{\bar{p}}(\epsilon, \vec{r}_{\mathrm{sol}})}{J_p(\epsilon, \vec{r}_{\mathrm{sol}})} = \left(\frac{J_{\bar{p}}(\epsilon, \vec{r}_{\mathrm{sol}})}{J_p(\epsilon, \vec{r}_{\mathrm{sol}})}\right)_{\mathrm{sec}} \times \left[1 + f_V \frac{Q_{\bar{p},\mathrm{DM}}(\epsilon, \vec{r}_{\mathrm{sol}})}{Q_{\bar{p},\mathrm{sec}}(\epsilon, \vec{r}_{\mathrm{sol}})}\right]. \tag{32}$$

The first factor on the right-hand side is the secondary antiproton to primary proton flux ratio. This quantity is constrained by the boron-to-carbon (B/C) data, leaving no free parameters. We conclude that, under some general assumptions, the antiproton to proton flux ratio including a DM contribution can be computed based on the relatively well-constrained local injection rates and only one additional parameter, f_V, encapsulating all the details of the propagation. A naive estimate suggests $f_V \sim L/h \sim$ 10–100, where $L \sim 1$–10 kpc is the assumed half-width of the CR propagation volume and $h \sim 100$ pc is the half-width of the Galactic gaseous disc.

The class of models for which Eq. (32) holds includes the disc + halo diffusion model with a homogeneous diffusion coefficient [96,97].[24] In Appendix B we use this model as a concrete example, deriving the precise realization of Eq. (32). We find, as expected, f_V in the range ~10–100, depending mainly on the size of the CR confinement halo with an order-one correction depending on the DM distribution.

[24]Of course, the class of models for which Eq. (32) holds includes also the well-known leaky box model [98].

In Fig. 7 we plot the antiproton to proton flux ratio with a DM component, corresponding to our benchmark models. The curves including the DM contribution are obtained by suppressing the pure background term to 75% of its central value (we find that a similar suppression also best describes the data with only the background component), and boosting the DM term by the factor SE $\times f_V$, indicated in the plot. The shaded region denotes a 40% uncertainty estimate for the background calculation [95]. Data points are taken from published [6] and preliminary [99] PAMELA data. As illustrated in Fig. 7, a future $\bar{p}$ signal can arise for $m_{\mathrm{DM}} \gtrsim 1$ TeV, with SE $\times f_V \gtrsim 10^3$. As a volume factor $f_V > 10$ is envisioned, the requirement on the Sommerfeld factor is SE $\gtrsim 100$, easy to obtain in our model with a 100 GeV radion. The TeV scale for the DM mass, roughly above which the resulting antiproton feature can be pushed higher than existing constraints to provide a future signal, is indicated by the vertical gold line of Fig. 4.

Concerning the astrophysical background calculation depicted in Fig. 7, a comment is in order. Extending the background prediction all the way to $E \sim$ TeV requires extrapolation of the CR grammage [provided in Appendix B, Eq. (B3)] beyond the range 200–300 GeV, where reliable data exist [100]. While there are indications that the grammage used in Fig. 7 persists to TeV energies [31], the issue is not currently settled [101]. We anticipate that with improved compositional CR data, extending to TeV energies, an updated model-independent prediction for the $\bar{p}/p$ ratio will become directly available along the

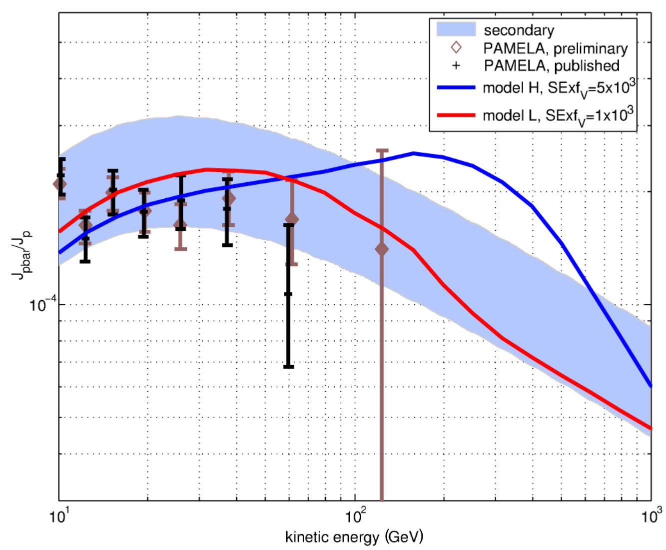

FIG. 7 (color online). The antiproton to proton flux ratio with a DM component, corresponding to our benchmark models. The curves including a DM contribution are obtained by suppressing the background prediction to 75% of its central value and boosting the local DM injection rate by a factor SE $\times f_V$. This factor encodes the combination of propagation, via the volume factor f_V, and of the SE. The shaded region indicates a 40% uncertainty estimate for the background calculation. Data points are from published and preliminary PAMELA data.

same lines described above [15,94,95]. Equation (32) will then become useful up to TeV energies.

5. Electrons, positrons, and the positron to antiproton flux ratio

Recently the PAMELA Collaboration has reported a rise in the positron to electron plus positron fraction [1], beginning at $E \sim 10$ GeV. The reported rise has induced numerous publications, suggesting an explanation in terms of DM annihilations or decay. However, before examining exotic contributions it is necessary to first understand the astrophysical background, which is harder to constrain than in the antiproton example.

In fact, since secondary positrons are produced by pp and spallation interactions, just like antiprotons, an upper bound to the positron flux can be obtained model independently, based on the measured CR grammage [15]. Contrasted with the data, this calculation reveals that the rising positron fraction is not accompanied by any actual positron excess with respect to the model-independent upper bound. One is forced to conclude that the rising positron fraction most likely corresponds to an unexpected spectral behavior of the suppression due to propagation energy losses, denoted here by f_s. Using the total $e^+ + e^-$ measurements [2,3,5,7] in conjunction with the PAMELA data, one finds $f_s \approx 0.3$ at $E \approx 10$ GeV, rising to $f_s \approx 1$ at the highest data bin $E \approx 80$ GeV. At $E \lesssim 40$ GeV, the suppression of the positron fraction can also be compared with the measured suppression due to the decay of the flux of radioactive unstable CR isotopes, such as ^{10}Be, ^{26}Al, and ^{36}Cl [97,102]. In particular, measurements of the (purely secondary) decaying charge to decayed charge Be/B extend to a rigidity of ≈ 40 GV [102]. These measurements suggest a value of $f_s \sim 0.3$ for positron energy $\sim$20 GeV, in agreement with the actual result and in support of the secondary origin of the detected positrons.

To summarize, it is our view that the rising positron fraction does not constitute an evidence for exotic components in the positron flux, simply because there does not seem to be any positron excess—merely an intriguing suppression pattern. If, however, future data released by the PAMELA mission or other experiments [30] establish that the rising behavior persists to $e^+/(e^+ + e^-) > 0.2$ beyond $\sim$100 GeV, a positron excess will indeed be implied, necessitating a primary source.

Neither of our benchmark models produce a hard lepton flux; hence, no anomaly is predicted in leptonic channels. This conclusion is supported by the expectation that, due to radiative losses, positrons do not experience the volume enhancement relevant for antiprotons. However, as argued above, since the background distribution (both of primary electrons and secondary electrons and positrons) is largely unknown, we proceed to discuss and analyze, in the following, a more robust observable related to secondary to secondary flux ratio.

In terms of theoretical uncertainties, the positron to antiproton flux ratio is a clean discriminator between a secondary astrophysical production mechanism and any other hypothetical source. The reason for this is that secondary antiprotons and positrons are produced by the same mechanism, namely, pp and spallation interactions of primary CRs with ISM. The relative amount of positrons and of antiprotons injected at a given energy depends on the corresponding branching ratios and, to a lesser extent, on the spectrum and composition of the primary CRs and the ISM. An examination of the dependence of the positron to antiproton ratio on the spectrum of primaries was carried out in [15], where this dependence was found to be very mild. Since at high energies energy losses affect only the positrons and act to suppress the observed flux, and since in the absence of losses high energy positrons and antiprotons would propagate in a similar way, the positron to antiproton injection rate ratio forms a robust upper bound on the corresponding flux ratio, relatively immune to propagation details.

The spectrum of final state products in DM annihilation may deviate significantly from the corresponding branching ratios in pp collisions. The existence of a DM component in the CR antimatter flux can therefore be searched for in the positron to antiproton flux ratio. Finding this ratio above the standard prediction (based essentially on the branching ratios in pp collisions, with mild compositional corrections) will provide strong motivation for an exotic contribution.

In Fig. 8 we plot the positron to antiproton production rate ratio for our benchmark models, including the background, compared with the prediction for pp collisions which can be regarded as an upper bound for the background result. In both models, the ratio lies very close to the astrophysical background. The conclusion is that it is

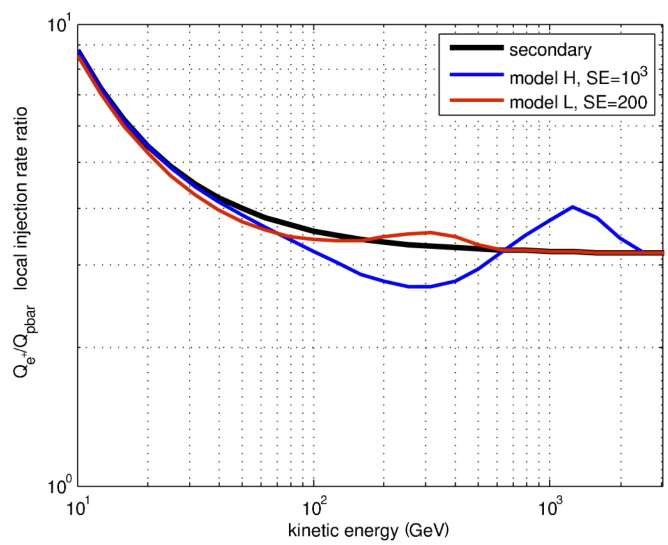

FIG. 8 (color online). Positron to antiproton production rate ratio.

unlikely, yet not inconceivable, that our models would lead to an excess in leptonic CR signals.

V. RADION COLLIDER PHENOMENOLOGY

For the region of our model parameter space, where a possible CR signal in DM annihilation is obtained, a lightish radion with mass in the 100 GeV range is required. This implies that the radion may turn out to be the lightest new particle in our model, likely to be accessible at the LHC. Various studies on radion phenomenology have been performed in the past [35–38,103–107], including recent works where radion dynamics was considered within realistic models of electroweak breaking with bulk SM fields [107–109]. For example, in the case of radion mass lighter than $2M_W$, $r \rightarrow \gamma\gamma$ is a promising channel [108], which can also be dramatically enhanced in the presence of Higgs-radion mixing [109]. For the case of radion mass larger than $2M_W$, WW, hh, ZZ,$t\bar{t}$ are the dominant channels which are expected to allow for a discovery at the LHC. Thus, a discovery of lightish radion at the LHC and future signals at CR experiments would yield support for our class of models.

VI. CONCLUSIONS

Indirect signals from DM annihilation in cosmic ray experiments have received renewed attention. We point out that models of warped extra dimension can naturally yield a low velocity enhancement of the DM annihilation via the Sommerfeld effect. The enhancement does not rely on an extra dark sector, but rather is mediated via an intrinsic component of the theory, namely, the radion with a mass at the hundred GeV range. More specifically, we studied the well-motivated framework of a warped grand unified theory (GUT, in which the DM particle is a GUT partner of the top quark. Based on the Pati-Salam group, we constructed models of partial and full unification, which accommodate custodial symmetry protection for $Z \rightarrow b\bar{b}$ coupling. The above construction is consistent with electroweak precision tests for Kaluza-Klein (KK) particles with a mass scale of a few TeV. In addition, we explored the consequences of a similar custodial symmetry protection of Z couplings to right-handed (RH) tau's. Such protection enables the RH tau's to be composite, localized near the TeV end of the extra dimension, hence having a large coupling to KK particles. As an aside, independently of the requirement for unification, the strong coupling between the KK particles and the composite tau's can lead to striking LHC signals.

Cosmological and astrophysical aspects of our framework are discussed. We find that the dark matter relic abundance, as well as direct detection, constrain the viable parameter space of this class of models. Particularly strong constraints are found in cases where the DM particle couples to the neutral electroweak sector. Indirect signatures in Galactic CRs are studied. We focus on robust observables, relatively immune to propagation model uncertainties, to test our framework. At present, we do not identify any clear evidence for exotic contributions. However, contrasted with upcoming data on the abundance of CR nuclei, near future measurements of the antiproton to proton flux ratio will provide a sharp probe for exotic contributions. Such contributions could naturally arise in our model. In the case where an indirect signal is observed, measurements of the radion and KK particle masses at the LHC collider will provide a nontrivial test of the model.

ACKNOWLEDGMENTS

We thank Zurab Berezhiani, Roberto Contino, Cédric Delaunay, Ben Gripaios, Andrey Katz, Boaz Katz, Frank Paige, Riccardo Rattazzi, Raman Sundrum, Tomer Volansky, Eli Waxman, and Jure Zupan for useful conversations. S. J. L. and G. P. also acknowledge the Galileo Galilei Institute for Theoretical Physics in Florence, Italy, where part of this work was completed. K. A. is supported in part by NSF Grant No. PHY-0652363. G. P. is supported by the Israel Science Foundation (Grant No. 1087/09) and EU-FP7 Marie Curie.

APPENDIX A: OTHER PATI-SALAM MODELS

We present two other models with custodial symmetry for $Zb\bar{b}$ coupling. Just like model I (a) presented in the main text, neither of these models seems to fit into $SO(10)$ representations smaller than **560** [64]. Moreover, even if we find a fit into a suitable larger representation of $SO(10)$, these models do not have $SU(5)$ normalization of hypercharge and hence might not be maintained even at the SM level of unification of gauge couplings.

1. Model I (b): $T_{3R}^{\nu'} \neq 0$ and custodial symmetry for leptons

In Table VIII, we first present a model with smaller $SU(4)_c$ representations than the benchmark model [where we had **35** of $SU(4)_c$]. This model has

$$Y = T_{3R} + \sqrt{\tfrac{8}{3}}X \tag{A1}$$

and hence $\sin^2\theta' = 3/11$. Also, this model has a larger value $T_{3R}^{\nu'} = 2$, but a smaller value of $\sin\theta'$ than the model with **35** of $SU(4)$. Such a modification tends to enhance the DM annihilation cross section via Z' exchange into Zh/WW, and similarly direct detection via Z exchange, whereas it reduces the annihilations via Z' exchange into top quarks (as per Table V).

2. Custodial symmetry only for b_L, but not leptons

Next, we present models with custodial representations only for b_L and not for RH leptons, with the following two motivations in mind. First of all, it is still interesting to

TABLE IX. Simplest model with custodial representation for b_L, but not for RH charged leptons: The subscripts denote the $\sqrt{8/3}$ X charge.

	$SU(4)_c \sim SU(3)_C \times U(1)_X$	$SU(2)_L$	$SU(2)_R$
t_R, ν'	$\mathbf{4} \sim \mathbf{3}_{(-1)/3}, \mathbf{1}_1 \ldots$	**1**	**5**
$(t, b)_L$	$\mathbf{4} \sim \mathbf{3}_{(-1)/3}, \ldots$	**2**	**4**
τ_R	$\mathbf{1} \sim \mathbf{1}_0$	**1**	**3**
$(\nu, \tau)_L$	$\mathbf{1} \sim \mathbf{1}_0$	**2**	**2**
b_R	$\mathbf{4} \sim \mathbf{3}_{(-1)/3}, \ldots$	**1**	**5**
H	**1**	**2**	**2**

have a scenario where RH leptons are not near the TeV brane and thus have small couplings to Z', so that we do not need custodial representations for them. In this case, DM annihilates mostly into a hadronic SM state; i.e., there is no e^+ signal. Moreover, we can achieve consistency with current $\bar{p}$ data, while simultaneously obtaining a $\bar{p}$ signal, by simply resorting to a smaller value of SE than needed in order to obtain e^+ signals (recall that with the larger SE, the large DM annihilation into leptons was doing a "-double-duty" of giving an e^+ signal and maintaining consistency with present $\bar{p}$ data).

Moreover, there are regions of parameter space where we cannot obtain signals from DM annihilation in cosmic rays, whether they are e^+ [even with enhanced couplings of Z' to (RH) leptons] or $\bar{p}$. For example, we can have heavy ($\sim$ TeV) DM as well as a heavy radion so that we do not have sufficient SE. Again, there is no motivation for custodial representations for RH leptons in this case. However, we still require custodial representations for $Zb\bar{b}$ so it is still interesting to build such a unified model.

Along these lines, the model with the smallest possible representations is given in Table IX, with

$$Y = T_{3R} - \sqrt{\frac{32}{3}}X \tag{A2}$$

and hence $\sin^2\theta' = 3/35$.

Also, this model has $T_{3R} = 2$ for ν' and hence is (roughly) similar to the above model with **10** of $SU(4)$ as far as relic density and direct detection are concerned.

APPENDIX B: THE VOLUME FACTOR FOR ANTIPROTON PROPAGATION: A DIFFUSION MODEL EXAMPLE

The disc + halo diffusion model for CR propagation is widely used in the literature (see e.g. [96]). In principle, the model allows one to compute the CR densities arising from standard astrophysical processes on the same footing as proposed exotic contributions, such as DM annihilation. In practice, the model parameters are tuned on compositional CR nuclei data, which only partially constrain them. Here we make use of this model for two purposes: (i) to clarify some issues regarding the currently fashionable "precision treatment" of exotic CR sources within a propagation-model-dependent framework, and (ii) to illustrate the volume enhancement factor for antiprotons from a DM annihilation source, described in Sect. IV C 4. Concerning the latter cause, we do not attribute particular significance to the precise numerical results, but rather consider them as order of magnitude estimates for the expected effect.

We consider a cylindrical halo model with an infinitely thin disc, taking the diffusion coefficient as spatially constant in the propagation volume with power-law energy dependence. The model parameters relevant in the high energy regime are L, the scale height of the cylinder; R, the radial extent; D_0, the normalization; and δ, the power-law index of the diffusion coefficient, given by $D(\epsilon) = D_0\epsilon^\delta$. The parameters L, R, D_0, δ are constrained by B/C data, in such a way as to provide the measured value of the CR grammage. For relativistic energies above a few GeV/nuc, this constraint can be summarized as follows,

$$X_{\rm esc}(\epsilon) \approx \frac{X_{\rm disc}Lc}{2D(\epsilon)} g(L, R). \tag{B1}$$

Above, $X_{\rm esc}$ is the CR grammage, $X_{\rm disc} \approx 200$ pc $\times$ $1.3m_p \times 1$ cm^{-3} $\approx 1.3 \times 10^{-3}$ gcm^{-2} is the column density of the gaseous disc, where spallation interactions occur, and c is the speed of light. The dimensionless correction factor $g(L, R)$ is given by

$$g(L, R) = \frac{2R}{L}\sum_{k=1}^{\infty} J_0\left(\nu_k \frac{\rho_{\rm sol}}{R}\right)\frac{\tanh(\nu_k \frac{L}{R})}{\nu_k^2 J_1(\nu_k)}, \tag{B2}$$

where ν_k are the zeros of the Bessel function of the first kind J_0. The correction factor obeys $g = 1$ for $L \ll R$, and becomes smaller than 1 if the distance of the solar system from the radial edge is taken to be comparable to the scale height of the cylinder. For the CR grammage we adopt the parametrization [110] (see also [100,111] for earlier estimates)

$$X_{\rm esc} = 27.5\epsilon^{-0.5} \text{ gcm}^{-2}. \tag{B3}$$

We present the CR grammage in Eqs. (B1) and (B3) as a function of energy $\epsilon = E/\text{GeV}$. In fact, the grammage depends rather on magnetic rigidity, $\mathcal{R} = pc/eZ$. The notation is consistent as long as we fix our attention on relativistic antiprotons.

From Eqs. (B1) and (B3) we can deduce the following relation,

$$D_0 \approx 2.9 \times 10^{-2}\left(\frac{L}{4\text{ kpc}}\right)\tilde{\epsilon}^{0.5-\delta} g(L, R) \text{ kpc}^2/\text{Myr}. \tag{B4}$$

Equation (B4) may now be used in order to define sets of parameters L, R, D_0, δ, which will agree with high energy B/C data as long as $\delta \sim 0.5$. To this end, any high energy value of $\tilde{\epsilon} \gtrsim 10$ GeV should do. We take $\tilde{\epsilon} =$ 75 GeV/nuc, corresponding to the highest energy B/C measurement by the HEAO3 mission [111,112]. The fact that propagation (and, in particular, diffusion) models must comply with the CR grammage is demonstrated, for example, by noting that Eq. (B4) holds very well for the popular MIN, MED, and MAX propagation models, defined in [113] after the work of [114].

Besides the CR grammage, additional information exists on the escape time scale, found from measurements of radioactive CR isotopes. These data are far less accurate than the grammage measurements, and are given only for a limited range of energies, mostly at the $\sim$100 MeV/nuc scale [97,102].

Different sets of values of L, R, D_0, δ, obeying Eq. (B4), are considered in the literature. However, we will see that, under realistic assumptions, the diffusion coefficient does not enter into the ratio between the antiproton flux arising from DM and from the astrophysical background. In fact, to a good approximation, the only parameter which controls this ratio is the scale height of the propagation volume. We note at this point that, as the scale height L is not independently constrained, the DM signal to astrophysical background ratio in the disc + halo model is not constrained by the B/C data. We now proceed to compute the flux of antiprotons resulting from DM annihilations in this propagation model example.

Neglecting losses and low energy processes and assuming a steady state, the diffusion equation is

$$-D(\epsilon)\nabla^2 n = Q_{\rm DM}, \tag{B5}$$

where n is the antiproton density. Neglecting losses made this equation easy to analyze, at the price of moderate imprecision at energies below a few tens of GeV. We will return to this point later. Because of the homogeneity of the diffusion coefficient, the energy dependence of the antiproton density follows that of the source, with a trivial softening resulting from the diffusion: $n(\epsilon, \vec{r}) = \epsilon^{-\delta} f(\vec{r}) Q(\epsilon, \vec{r})$. We are left to deal with the spatial dependence, consisting of the function $f(\vec{r})$ for which we need to derive the value in the vicinity of the solar system.

Decomposing both n and Q in the Bessel-Fourier series reduces the problem to an infinite set of leaky box model-like [96] equations for the coefficients. We chose a decomposition in basis functions which automatically satisfy the boundary conditions of vanishing CR density on the surface of the cylinder. For the DM source, the decomposition reads

$$\begin{aligned} Q_{mk}(\epsilon) &= \frac{4}{J_1^2(\nu_k)} \int_0^1 d\zeta \cos\left[\pi\zeta\left(m + \frac{1}{2}\right)\right] \\ &\quad \times \int_0^1 d\eta\, \eta J_0(\nu_k \eta) Q_{\rm DM}(\epsilon, z = \zeta L, \rho = \eta R), \\ Q_{\rm DM}(\epsilon, \vec{r}) &= \sum_{m=0}^{\infty} \sum_{k=1}^{\infty} Q_{mk}(\epsilon) J_0\left(\nu_k \frac{\rho}{R}\right) \cos\left[\frac{\pi z}{L}\left(m + \frac{1}{2}\right)\right]. \end{aligned} \tag{B6}$$

A similar decomposition holds for the antiproton density with the replacement $Q_{mk} \leftrightarrow n_{mk}$. Using (B5) we then have, for the coefficients of the antiproton density,

$$n_{mk}(\epsilon) = \frac{Q_{mk}(\epsilon) L^2}{D(\epsilon)} \left[\pi^2\left(m + \frac{1}{2}\right)^2 + \nu_k^2 \frac{L^2}{R^2}\right]^{-1}. \tag{B7}$$

Note that the DM source is separable,

$$\begin{aligned} Q_{\rm DM}(\vec{r}) &= Q_{{\rm DM},\bar{p}}(\epsilon, \vec{r}_{\rm sol}) n_o^2(\vec{r}), \\ Q_{mk}(\epsilon) &= Q_{{\rm DM},\bar{p}}(\epsilon, \vec{r}_{\rm sol}) q_{mk}, \end{aligned} \tag{B8}$$

with q_{mk} the Bessel-Fourier coefficients of $n_o^2(\vec{r})$. [Recall that $n_o(\vec{r})$ is defined as the DM number density normalized to its value in the vicinity of the solar system, such that $Q_{{\rm DM},\bar{p}}(\epsilon, \vec{r}_{\rm sol})$ is just the local injection rate due to DM.] The antiproton density in the solar neighborhood, $z = 0$, $\rho = r_{\rm sol}$, is thus

$$n(\epsilon, \vec{r}_{\rm sol}) = \frac{aL^2}{D(\epsilon)} Q_{\rm DM}(\epsilon, \vec{r}_{\rm sol}), \tag{B9}$$

with

$$a = \sum_{m=0}^{\infty} \sum_{k=1}^{\infty} \frac{q_{mk} J_0(\nu_k \frac{\rho_{\rm sol}}{R})}{\pi^2 (m + \frac{1}{2})^2 + \nu_k^2 \frac{L^2}{R^2}}. \tag{B10}$$

Equation (B9) allows us to obtain the specific value of the volume factor by which the DM annihilation source is enhanced in comparison with the production by spallation. Again neglecting losses, the antiproton density near the solar system, resulting from spallation, is [15]

$$n_{\bar{p},{\rm spal}} = \frac{X_{\rm esc}}{\rho_{\rm ISM} c} Q_{{\rm spal},\bar{p}}, \tag{B11}$$

where $\rho_{\rm ISM} \approx 1.3 m_p$ cm^{-3} is the matter density on the disc. Using Eq. (B1) and noting that $X_{\rm disc} \approx 2h\rho_{\rm ISM}$, where $h \sim 100$ pc is the half-width of the disc, we obtain the ratio of the local antiproton density due to DM annihilation and due to spallation throughout the Galaxy, expressed in terms of the local injection rates:

$$\frac{n_{\bar{p},{\rm DM}}}{n_{\bar{p},{\rm spal}}} = f_V \frac{Q_{{\rm DM},\bar{p}}(\epsilon, \vec{r}_{\rm sol})}{Q_{{\rm spal},\bar{p}}(\epsilon, \vec{r}_{\rm sol})}, \quad \text{with} \quad f_V = \frac{aL}{gh}. \tag{B12}$$

On the left panel of Fig. 9 we plot the ratio of the two dimensionless correction factors a/g as a function of the CR halo half-width L. We consider three DM halo profiles: the cored isothermal (ISO) and the cusped NFW, defined in Sec. IV C 2, and the Einasto profile [115]. The ratio a/g is of order unity, larger for cuspy profiles compared with the cored one. To achieve faster convergence, we have regulated the inner cusp in the NFW and Einasto distributions by assuming flat DM density for $r < 200$ pc. Such an inner radius is not constrained by N-body simulations. We have verified that our results do not vary significantly as a result of increasing the regulation radius. On the right panel we plot the resulting volume enhancement factor aL/gh for $h = 100$ pc. We find that, for reasonable values of L, the

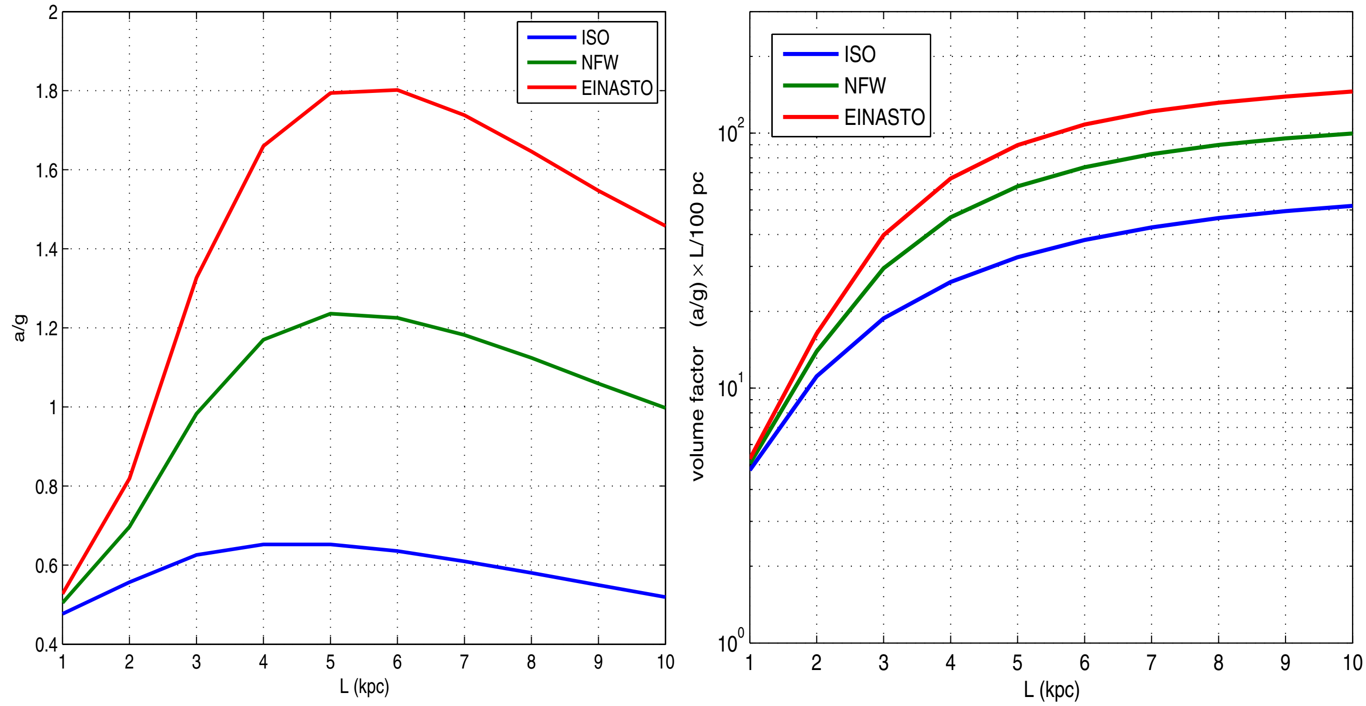

FIG. 9 (color online). Left panel: The ratio between the geometrical correction factors a and g, defined in the text. Right panel: The volume enhancement factor for the DM annihilation source over the spallation source. In both panels we keep $R = 20$ kpc fixed. On the right, we take $h = 100$ pc for the half-width of the gaseous disc.

volume factor is in the range $f_V \sim 10$–100, depending on the assumed DM halo profile.

We now comment on the neglect of losses in the discussion above. For spallation antiprotons, the error due to neglecting losses diminishes with increasing energy, as a result of the relatively rapid decrease in the grammage. For example, the errors contained in Eq. (B11) due to the neglect of losses are $\approx 25\%$, 10%, and 5% at antiproton energies of 10, 30, and 100 GeV, respectively. Regarding the antiprotons from DM annihilation, the conclusion may be model dependent. However, in the diffusion model considered above (as well as e.g. in the leaky box model), the escape time shares the energy dependence of the grammage, and the conclusion is similar to the background case. In addition to losses by collisions with ambient matter, other low energy processes are expected to influence the calculation below a few tens of GeV. These phenomena include solar modulation, ionization losses, and even possible reacceleration or convective motion [97]. As we are dealing with a simplified propagation model which involves, for example, *ad hoc* boundary conditions for the CR halo and diffusion coefficient, and an uncertain DM halo distribution, we find it useful to keep our expressions tractable and accurate at the high energy, $\gtrsim 50$ GeV, regime, at the cost of minor accuracy loss below a few tens of GeV.

[1] O. Adriani *et al.* (PAMELA Collaboration), Nature (London) **458**, 607 (2009).
[2] J. Chang *et al.*, Nature (London) **456**, 362 (2008).
[3] A. A. Abdo *et al.* (Fermi LAT Collaboration), Phys. Rev. Lett. **102**, 181101 (2009).
[4] F. Aharonian *et al.* (H.E.S.S. Collaboration), Phys. Rev. Lett. **101**, 261104 (2008).
[5] M. A. DuVernois *et al.*, Astrophys. J. **559**, 296 (2001).
[6] M. Boezio *et al.*, arXiv:0810.3508.
[7] J. Alcaraz *et al.* (AMS Collaboration), Phys. Lett. B **484**, 10 (2000); **495**, 440(E) (2000).
[8] S. W. Barwick *et al.* (HEAT Collaboration), Astrophys. J. **482**, L191 (1997).
[9] S. Torii *et al.*, Astrophys. J. **559**, 973 (2001).
[10] S. Torii *et al.* (PPB-BETS Collaboration), arXiv:0809.0760.
[11] H. E. S. Aharonian, arXiv:0905.0105.
[12] A. Morselli and I. V. Moskalenko, Proc. Sci., IDM2008 (2008) 025 [arXiv:0811.3526].
[13] T. Delahaye, F. Donato, N. Fornengo, J. Lavalle, R. Lineros, P. Salati, and R. Taillet, Astron. Astrophys. **501**, 821 (2009).

[14] M. Schubnell, arXiv:0905.0444.
[15] B. Katz, K. Blum, and E. Waxman, arXiv:0907.1686.
[16] T. Delahaye, R. Lineros, F. Donato, N. Fornengo, and P. Salati, Phys. Rev. D **77**, 063527 (2008).
[17] P. Blasi, Phys. Rev. Lett. **103**, 051104 (2009).
[18] R. Cowsik and B. Burch, arXiv:0905.2136; arXiv:0906.2365.
[19] N. J. Shaviv, E. Nakar, and T. Piran, Phys. Rev. Lett. **103**, 111302 (2009).
[20] A. M. Atoian, F. A. Aharonian, and H. J. Volk, Phys. Rev. D **52**, 3265 (1995); I. Büshing *et al.*, arXiv:0804.0220; T. Kobayashi, Y. Komori, K. Yoshida, and J. Nishimura, Astrophys. J. **601**, 340 (2004); arXiv:astro-ph/0308470; D. Hooper, P. Blasi, and P. D. Serpico, J. Cosmol. Astropart. Phys. 01 (2009) 025; H. Yuksel, M. D. Kistler, and T. Stanev, Phys. Rev. Lett. **103**, 051101 (2009); P. D. Serpico, Phys. Rev. D **79**, 021302 (2009); S. Profumo, arXiv:0812.4457.
[21] I. Cholis, G. Dobler, D. P. Finkbeiner, L. Goodenough, and N. Weiner, Phys. Rev. D **80**, 123518 (2009).
[22] M. Cirelli, M. Kadastik, M. Raidal, and A. Strumia, Nucl. Phys. **B813**, 1 (2009); M. Cirelli and A. Strumia, arXiv:0808.3867.
[23] N. Arkani-Hamed, D. P. Finkbeiner, T. R. Slatyer, and N. Weiner, Phys. Rev. D **79**, 015014 (2009).
[24] D. Hooper, arXiv:0901.4090.
[25] X. G. He, Mod. Phys. Lett. A **24**, 2139 (2009).
[26] A. Sommerfeld, Ann. Phys. (Leipzig) **403**, 257 (1931); J. Hisano, S. Matsumoto, and M. M. Nojiri, Phys. Rev. Lett. **92**, 031303 (2004); J. Hisano, S. Matsumoto, M. M. Nojiri, and O. Saito, Phys. Rev. D **71**, 015007 (2005).
[27] D. Feldman, Z. Liu, and P. Nath, Phys. Rev. D **79**, 063509 (2009).
[28] M. Ibe, H. Murayama, and T. T. Yanagida, Phys. Rev. D **79**, 095009 (2009).
[29] D. Hooper, A. Stebbins, and K. M. Zurek, Phys. Rev. D **79**, 103513 (2009).
[30] B. Alpat, arXiv:astro-ph/0308487.
[31] H. S. Ahn *et al.*, Astropart. Phys. **30**, 133 (2008).
[32] L. Randall and R. Sundrum, Phys. Rev. Lett. **83**, 3370 (1999).
[33] Y. Bai, M. Carena, and J. Lykken, Phys. Rev. Lett. **103**, 261803 (2009).
[34] W. D. Goldberger and M. B. Wise, Phys. Rev. Lett. **83**, 4922 (1999).
[35] W. D. Goldberger and M. B. Wise, Phys. Lett. B **475**, 275 (2000).
[36] C. Csáki, M. Graesser, L. Randall, and J. Terning, Phys. Rev. D **62**, 045015 (2000).
[37] O. DeWolfe, D. Z. Freedman, S. S. Gubser, and A. Karch, Phys. Rev. D **62**, 046008 (2000).
[38] T. Tanaka and X. Montes, Nucl. Phys. **B582**, 259 (2000).
[39] C. Csaki, M. L. Graesser, and G. D. Kribs, Phys. Rev. D **63**, 065002 (2001).
[40] J. Garriga and A. Pomarol, Phys. Lett. B **560**, 91 (2003).
[41] K. Agashe and G. Servant, Phys. Rev. Lett. **93**, 231805 (2004); J. Cosmol. Astropart. Phys. 02 (2005) 002.
[42] K. Agashe, A. Falkowski, I. Low, and G. Servant, J. High Energy Phys. 04 (2008) 027.
[43] G. Panico, E. Ponton, J. Santiago, and M. Serone, Phys. Rev. D **77**, 115012 (2008); Y. Cui, D. E. Morrissey, D. Poland, and L. Randall, J. High Energy Phys. 05 (**2009**) 076.
[44] K. Agashe, R. Contino, L. Da Rold, and A. Pomarol, Phys. Lett. B **641**, 62 (2006).
[45] See, for example, K. Agashe, A. Delgado, and R. Sundrum, Ann. Phys. (N.Y.) **304**, 145 (2003).
[46] K. Agashe, R. Contino, and R. Sundrum, Phys. Rev. Lett. **95**, 171804 (2005).
[47] D. Hooper and G. Servant, Astropart. Phys. **24**, 231 (2005); C. B. Jackson, G. Servant, G. Shaughnessy, T. M. P. Tait, and M. Taoso, arXiv:0912.0004.
[48] H. Baer and S. Profumo, J. Cosmol. Astropart. Phys. 12 (2005) 008.
[49] H. Davoudiasl, S. Gopalakrishna, E. Ponton, and J. Santiago, arXiv:0908.1968.
[50] R. Contino, Y. Nomura, and A. Pomarol, Nucl. Phys. **B671**, 148 (2003).
[51] J. M. Maldacena, Adv. Theor. Math. Phys. **2**, 231 (1998); Int. J. Theor. Phys. **38**, 1113 (1999); S. S. Gubser, I. R. Klebanov, and A. M. Polyakov, Phys. Lett. B **428**, 105 (1998); E. Witten, Adv. Theor. Math. Phys. **2**, 253 (1998).
[52] N. Arkani-Hamed, M. Porrati, and L. Randall, J. High Energy Phys. 08 (2001) 017; R. Rattazzi and A. Zaffaroni, J. High Energy Phys. 04 (2001) 021; A. Pomarol, Phys. Lett. B **486**, 153 (2000); S. Chang, J. Hisano, H. Nakano, N. Okada, and M. Yamaguchi, Phys. Rev. D **62**, 084025 (2000).
[53] Y. Grossman and M. Neubert, Phys. Lett. B **474**, 361 (2000).
[54] T. Gherghetta and A. Pomarol, Nucl. Phys. **B586**, 141 (2000).
[55] A. Delgado, A. Pomarol, and M. Quiros, J. High Energy Phys. 01 (2000) 030.
[56] S. J. Huber and Q. Shafi, Phys. Lett. B **498**, 256 (2001).
[57] K. Agashe, G. Perez, and A. Soni, Phys. Rev. D **71**, 016002 (2005); Phys. Rev. Lett. **93**, 201804 (2004).
[58] C. Csaki, G. Perez, Z. Surujon, and A. Weiler, arXiv:0907.0474.
[59] O. Gedalia, G. Isidori, and G. Perez, Phys. Lett. B **682**, 200 (2009); K. Agashe, A. Azatov, and L. Zhu, Phys. Rev. D **79**, 056006 (2009); C. Csaki, A. Falkowski, and A. Weiler, J. High Energy Phys. 09 (2008) 008; S. Davidson, G. Isidori, and S. Uhlig, Phys. Lett. B **663**, 73 (2008); M. Blanke, A. J. Buras, B. Duling, S. Gori, and A. Weiler, J. High Energy Phys. 03 (2009) 001; M. Bauer, S. Casagrande, U. Haisch, and M. Neubert, arXiv:0912.1625.
[60] C. Csaki and D. Curtin, Phys. Rev. D **80**, 015027 (2009); C. Csaki, A. Falkowski, and A. Weiler, Phys. Rev. D **80**, 016001 (2009); J. Santiago, J. High Energy Phys. 12 (2008) 046; M. C. Chen, K. T. Mahanthappa, and F. Yu, Phys. Rev. D **81**, 036004 (2010); A. L. Fitzpatrick, L. Randall, and G. Perez, Phys. Rev. Lett. **100**, 171604 (2008); G. Perez and L. Randall, J. High Energy Phys. 01 (2009) 077; M. C. Chen and H. B. Yu, Phys. Lett. B **672**, 253 (2009); C. Csaki, C. Delaunay, C. Grojean, and Y. Grossman, J. High Energy Phys. 10 (2008) 055; G. Cacciapaglia, C. Csaki, J. Galloway, G. Marandella, J. Terning, and A. Weiler, J. High Energy Phys. 04 (2008) 006.
[61] K. Agashe, A. Delgado, M. J. May, and R. Sundrum, J. High Energy Phys. 08 (2003) 050.

[62] B. Gripaios, J. High Energy Phys. 02 (2010) 045.
[63] LEP Collaboration, arXiv:hep-ex/0312023, see Table 8.14.
[64] See e.g. R. Slansky, Phys. Rep. **79**, 1 (1981).
[65] Ben Gripaios (private communication).
[66] P. Belli, R. Cerulli, N. Fornengo, and S. Scopel, Phys. Rev. D **66**, 043503 (2002).
[67] F. Governato *et al.*, Mon. Not. R. Astron. Soc. **374**, 1479 (2007).
[68] J. L. Feng, M. Kaplinghat, and H. B. Yu, arXiv:0911.0422.
[69] M. R. Buckley and P. J. Fox, arXiv:0911.3898.
[70] G. Belanger, F. Boudjema, A. Pukhov, and A. Semenov, Comput. Phys. Commun. **176**, 367 (2007).
[71] K. Agashe *et al.*, Phys. Rev. D **76**, 115015 (2007).
[72] H. Davoudiasl, J. L. Hewett, and T. G. Rizzo, Phys. Rev. D **68**, 045002 (2003); M. Carena, E. Ponton, T. M. P. Tait, and C. E. M. Wagner, Phys. Rev. D **67**, 096006 (2003); M. S. Carena, A. Delgado, E. Ponton, T. M. P. Tait, and C. E. M. Wagner, Phys. Rev. D **68**, 035010 (2003).
[73] See, for example, discussion below Eq. (12) in S. Gopalakrishna, S. J. Lee, and J. D. Wells, Phys. Lett. B **680**, 88 (2009).
[74] H. Davoudiasl, G. Perez, and A. Soni, Phys. Lett. B **665**, 67 (2008); G. Cacciapaglia, C. Csaki, G. Marandella, and J. Terning, Phys. Rev. D **75**, 015003 (2007); J. Thaler and I. Yavin, J. High Energy Phys. 08 (2005) 022; M. Piai, arXiv:0704.2205.
[75] G. Belanger, A. Pukhov, and G. Servant, J. Cosmol. Astropart. Phys. 01 (2008) 009.
[76] A. Bottino, F. Donato, N. Fornengo, and S. Scopel, Phys. Rev. D **72**, 083521 (2005).
[77] G. Belanger, F. Boudjema, A. Pukhov, and A. Semenov, Comput. Phys. Commun. **180**, 747 (2009).
[78] For the Xenon project see E. Aprile *et al.*, Nucl. Phys. B, Proc. Suppl. **138**, 156 (2005); For the SuperCDMS project see P. L. Brink *et al.* (CDMS-II Collaboration), arXiv: astro-ph/0503583.
[79] B. Robertson and A. Zentner, Phys. Rev. D **79**, 083525 (2009).
[80] E. Romano-Diaz, I. Shlosman, Y. Hoffman, and C. Heller, arXiv:0808.0195.
[81] J. A. Sellwood, arXiv:0807.1973.
[82] J. F. Navarro, C. S. Frenk, and S. D. M. White, Astrophys. J. **462**, 563 (1996).
[83] J. N. Bahcall and R. M. Soneira, Astrophys. J. Suppl. Ser. **44**, 73 (1980).
[84] F. Aharonian *et al.* (H.E.S.S. Collaboration), Phys. Rev. Lett. **97**, 221102 (2006); **97**, 249901(E) (2006).
[85] F. Aharonian *et al.* (H.E.S.S. Collaboration), Nature (London) **439**, 695 (2006).
[86] F. Aharonian *et al.* (H.E.S.S. Collaboration), Astron. Astrophys. **432**, L25 (2005).
[87] S. Murgia (Fermi-LAT), Proceedings of TeV Particle Astrophysics (TeVPA), 2009.
[88] S. Desai *et al.* (Super-Kamiokande Collaboration), Phys. Rev. D **70**, 083523 (2004); **70**, 109901(E) (2004).
[89] J. Mardon, Y. Nomura, D. Stolarski, and J. Thaler, J. Cosmol. Astropart. Phys. 05 (2009) 016.
[90] M. Papucci and A. Strumia, J. Cosmol. Astropart. Phys. 03 (2010) 014.
[91] M. Cirelli, P. Panci, and P. D. Serpico, arXiv:0912.0663.
[92] P. Meade, M. Papucci, and T. Volansky, J. High Energy Phys. 12 (2009) 052.
[93] A. Bottino, F. Donato, N. Fornengo, and P. Salati, Phys. Rev. D **58**, 123503 (1998); J. L. Feng, K. T. Matchev, and F. Wilczek, Phys. Rev. D **63**, 045024 (2001); A. Barrau, G. Boudoul, F. Donato, D. Maurin, P. Salati, and R. Taillet, Astron. Astrophys. **388**, 676 (2002); F. Donato, N. Fornengo, D. Maurin, and P. Salati, Phys. Rev. D **69**, 063501 (2004); A. Barrau, P. Salati, G. Servant, F. Donato, J. Grain, D. Maurin, and R. Taillet, Phys. Rev. D **72**, 063507 (2005).
[94] T. K. Gaisser and R. K. Schaefer, Astrophys. J. **394**, 174 (1992).
[95] M. Simon, A. Molnar, and S. Roesler, Astrophys. J. **499**, 250 (1998).
[96] V. L. Ginzburg, V. A. Dogiel, V. S. Berezinsky, S. V. Bulanov, and V. S. Ptuskin, *Astrophysics of Cosmic Rays* (North-Holland, Amsterdam, Netherlands, 1990), p. 534; V. L. Ginzburg and V. S. Ptuskin, Rev. Mod. Phys. **48**, 161 (1976); **48**, 675(E) (1976).
[97] A. W. Strong, I. V. Moskalenko, and V. S. Ptuskin, Annu. Rev. Nucl. Part. Sci. **57**, 285 (2007).
[98] R. Schlickeiser and I. Lerche, NASA. Goddard Space Flight Center 19th International Cosmic Ray Conference, Vol. 3, p. 54.
[99] P. Picozza (PAMELA), Proceedings of TeV Particle Astrophysics (TeVPA), 2009.
[100] J. J. Engelmann, P. Ferrando, A. Soutoul, P. Goret, and E. Juliusson, Astron. Astrophys. **233**, 96 (1990).
[101] V. I. Zatsepin *et al.*, arXiv:0905.0049.
[102] W. R. Webber and A. Soutoul, Astrophys. J. **506**, 335 (1998).
[103] G. F. Giudice, R. Rattazzi, and J. D. Wells, Nucl. Phys. **B595**, 250 (2001).
[104] C. Csáki, M. L. Graesser, and G. D. Kribs, Phys. Rev. D **63**, 065002 (2001).
[105] D. Dominici, B. Grzadkowski, J. F. Gunion, and M. Toharia, Nucl. Phys. **B671**, 243 (2003); J. F. Gunion, M. Toharia, and J. D. Wells, Phys. Lett. B **585**, 295 (2004).
[106] S. Bae, P. Ko, H. S. Lee, and J. Lee, arXiv:hep-ph/0103187.
[107] T. G. Rizzo, J. High Energy Phys. 06 (2002) 056.
[108] C. Csaki, J. Hubisz, and S. J. Lee, Phys. Rev. D **76**, 125015 (2007).
[109] M. Toharia, Phys. Rev. D **79**, 015009 (2009); A. Azatov, M. Toharia, and L. Zhu, Phys. Rev. D **80**, 031701 (2009).
[110] W. R. Webber, F. B. McDonald, and A. Lukasiak, Astrophys. J. **599**, 582 (2003).
[111] F. C. Jones, A. Lukasiak, V. Ptuskin, and W. Webber, Astrophys. J. **547**, 264 (2001).
[112] S. A. Stephens and R. E. Straitmatter, Astrophys. J. **505**, 266 (1998).
[113] F. Donato, N. Fornengo, D. Maurin, and P. Salati, Phys. Rev. D **69**, 063501 (2004).
[114] D. Maurin, F. Donato, R. Taillet, and P. Salati, Astrophys. J. **555**, 585 (2001).
[115] D. Merritt, J. F. Navarro, A. Ludlow, and A. Jenkins, Astrophys. J. **624**, L85 (2005).